Geological Solutions for Providing a Scientific Basis for Differing Site Condition Claims

Charles Merguerian, Duke Geological Laboratory, 55 Spongia Road, Stone Ridge, NY 12484, (845) 687-6386; CharlesM@Dukelabs.com
J. Mickey Merguerian, Dukelabs DSC, Inc., 16 Middle Lane, Westbury, NY 11590; (917) 805-3072; Mick@Dukelabs.com

Abstract

As an adjunct to construction risk assessment and to establish as-built claim recoveries over the years, we have applied many simple geological techniques to evaluate a broad array of anomalous subsurface conditions that resulted in impeded production rates and expanded construction costs throughout the NYC metropolitan region. These issues were detected in varied geological terrains for both tunnel boring machine (TBM) and traditional drill and blast tunnel excavations, large-diameter vertical shafts and smaller-diameter caisson and pile installations. The natural subsurface conditions resulted in costly remediation efforts and prolonged differing site condition (DSC) claims where unanticipated underlying geological causes resulted in low penetration rates, short stand-up times, water and material inflows, sidewall- and crown collapse and invert heave. Job-suspending excessive inflows of water and materials during drilling of vertical shafts were also experienced at various locations.

Although we can not disclose exact locations of these endeavors, we can share the geological techniques that have allowed us to provide a scientific basis for successful differing site condition claim representation. All of these cases depended upon documenting anomalous actual (as-built) conditions compared to those anticipated by bidding contractors based on provided pre-bid geotechnical information. Based on site type, our directed techniques encompassed traditional mapping and structural analysis including three-point problem solutions, lithologic- and petrographic studies to determine mineralogy, texture and metamorphic grade controls, rock mass density studies, comparative studies involving pre-bid borings vs. as-built Recovery (REC %) and Rock Quality Designation (RQD %) along with unconfined compressive stress (UCS) analysis and controlled subsurface video efforts resulting in 3-D mapping of subaqueous shafts of bridge piers in standing water locations.

Together, such directed geological techniques have proved crucial for both owners and contractors in providing a testable, scientific basis for defining departures from pre-bid anticipated subsurface rock mass conditions.

Introduction

Subsurface construction efforts such as drill and blast and TBM tunnels, drilled small diameter caissons (generally up to 10’ diameter) and large-diameter (>10’) shafts can generate construction difficulties. Hitherto unknown natural geological conditions can create costly delays because of short stand-up times of sidewalls and crowns and inflows of water +/- materials. These events always cause budget overruns and often result in contentious DSC claims. Owner’s arguments usually revolve around the accusation of use of improper means and methods by the contractor while contractors strive to demonstrate that a material change in

subsurface conditions exists compared to their reasonable anticipation based on pre-bid documents. In theory the federally mandated DSC clause in sealed bid contracts levels the playing field by eliminating excessive built-in costs for unknown risk. Unfortunately, trained professional geotechnical specialists familiar with the region in question are seldom employed at the pre-bid stage to outline potential risk so dispute resolution boards and litigation often result at the end-of-job.

Since 1975 as consultants for both contractors and owners in the building trades we have represented clients by recording the scientific basis for or against claims and have used some basic geological investigative techniques in support or denial of such claims. Here, without specifically identifying any individual job site nor client, we share some techniques employed for such construction efforts. Below we discuss three of our efforts in client support for subaqueous bridge shafts, terrestrial drilling of caissons for building support and TBM tunnel excavations.

Subaqueous Bridge Shafts

The first investigation we would like to share concerns a site in the Mesozoic Newark Basin of New Jersey (Figure 1). This consult involved difficulty in drilling 96" shafts within a gently inclined sedimentary rock unit that underlies bridge piers constructed across a river environment. Here, high-water inflows, overnight infilling of casings to base level and infalling blocks of rock plagued the effort and some aquatic life (an eel) was detected in one of the shafts. Abiding by the environmental principle promoted by our dear friend the late Dr. John E. Sanders that *"the fish never lose in court"*, we were interested in the consult and ultimately engaged.

Figure 1 - Physiographic diagram showing the eight major geological provinces in southern New York, northern New Jersey and adjoining states of PA, CT and MA. (From Bennington and Merguerian 2007.)

Construction Problems with Boulders and High-Water Inflows

During construction of the bridge, 45 shafts of 96” diameter were drilled for bridge piers using identical means and methods and finished with 90” rock sockets. Difficulties in construction were encountered in drilling eight of the river shafts. In these instances, shaft construction was hindered by voids, high-water inflows and in-falling blocks of red-colored siltstone and sandstone. The ground conditions required remediation including grouting, additional drilling, reseating of casings and deepening of shafts. A view of the equipment used for subaqueous drilling is shown below (Figure 2).

Figure 2 – Westward view of Shaft #23 construction rig near Pier 3 of job site in New Jersey (L) and close-up view of the cutterhead and cutters (R) designed for sedimentary rocks. (Dukelabs digital images taken 14 June 2013.)

The boulders mucked from within Shaft #23 examined on-site were sub-angular in shape and somewhat tabular, partially smoothed and consisted of Mesozoic Passaic Formation sandstone and siltstone (Figure 3). Notably, although somewhat similar in appearance to glacial boulders, they exhibited curved scratches indicating circular transport and grooving not the straight parallel striae associated with glacial activity. In addition, the boulders did not show the characteristic sub-rounded to rounded shape nor polish glacial boulders and were not exotic but consisted of rock types that are indigenous to the Passaic Formation which underlies the site. One boulder showed parallel joint surfaces outlined with greenish-white mineralization (chlorite+quartz infilling) suggesting the presence of subsurface fractures (joints and/or faults).

Based on the presence of mineralized joints, sub-angular/tabular shape aspect, and curved scratches, our conclusion was that the boulders were locally harvested (not of glacial origin), introduced from the shaft walls during drilling of fractured ground and dragged about during the drilling or mucking process before they were removed from the base of the shaft. Boulder composition was an identical match with the local Passaic bedrock. They were not Paleozoic quartzite or limestone which had been reported as indigenous boulders from within the Passaic

Formation by other field workers. Indeed, these observations forced the conclusion that the boulders were introduced from the shaft walls during construction drilling.

Figure 3 – View of subangular boulders and cobbles of Passaic Formation siltstone and sandstone mucked from base of Shaft #23. Note the tabular aspect of the boulders, a relic of original bedding, and the incipient polishing by mechanical means. Hammer is 38 cm (15") in length. (Dukelabs digital image taken 14 June 2013.)

High water inflows and blow-ins were also experienced during the drilling. Such inflows could only indicate sub-casing lip hydrologic connectivity to the adjacent river. The presence of intersecting open joints and/or faults are the typical explanations for such phenomenon in this type of shallow subsurface construction setting. Our video surveys and mapping verified this concept, as discussed below.

We were retained by the contractor to review drilling difficulties and slowdowns during 2010 -2012 for shafts at the bridge pier sites wherein sidewall instabilities and excessive inflows of water and sediment proved an impediment to efficient construction. In all, eight (8) out of 45 drilled shafts (17.8%) experienced a similar DSC. A site map of the three of six bridge piers (Piers 1, 2 and 3) affected by such issues is shown as Figure 4.

Stratigraphy and Lithology of the Bedrock

A full review of the geological literature yielded pertinent information. Geological maps show that the rock unit that underlies the job site is the Passaic Formation of the Newark Supergroup (Olson 1980a, b, c) which consists of a thick (3,550 m) gently NW-tilted sedimentary rock sequence of interlayered red-colored siltstone, shale, and sandstone of

Mesozoic age and intercalated basalt flows and intrusives. These igneous rocks and bounding sedimentary strata were originally deposited horizontally but now dip gently toward the NW at about 10° to 15°, depending upon one's position in the basin. Some stratigraphic horizons, particularly near the Ramapo basin-marginal fault, contain well-rounded boulders and cobbles of much older Paleozoic rock (typically quartzite and carbonate) eroded from uplift of such rocks formerly found above the adjacent Proterozoic Hudson Highlands terrain.

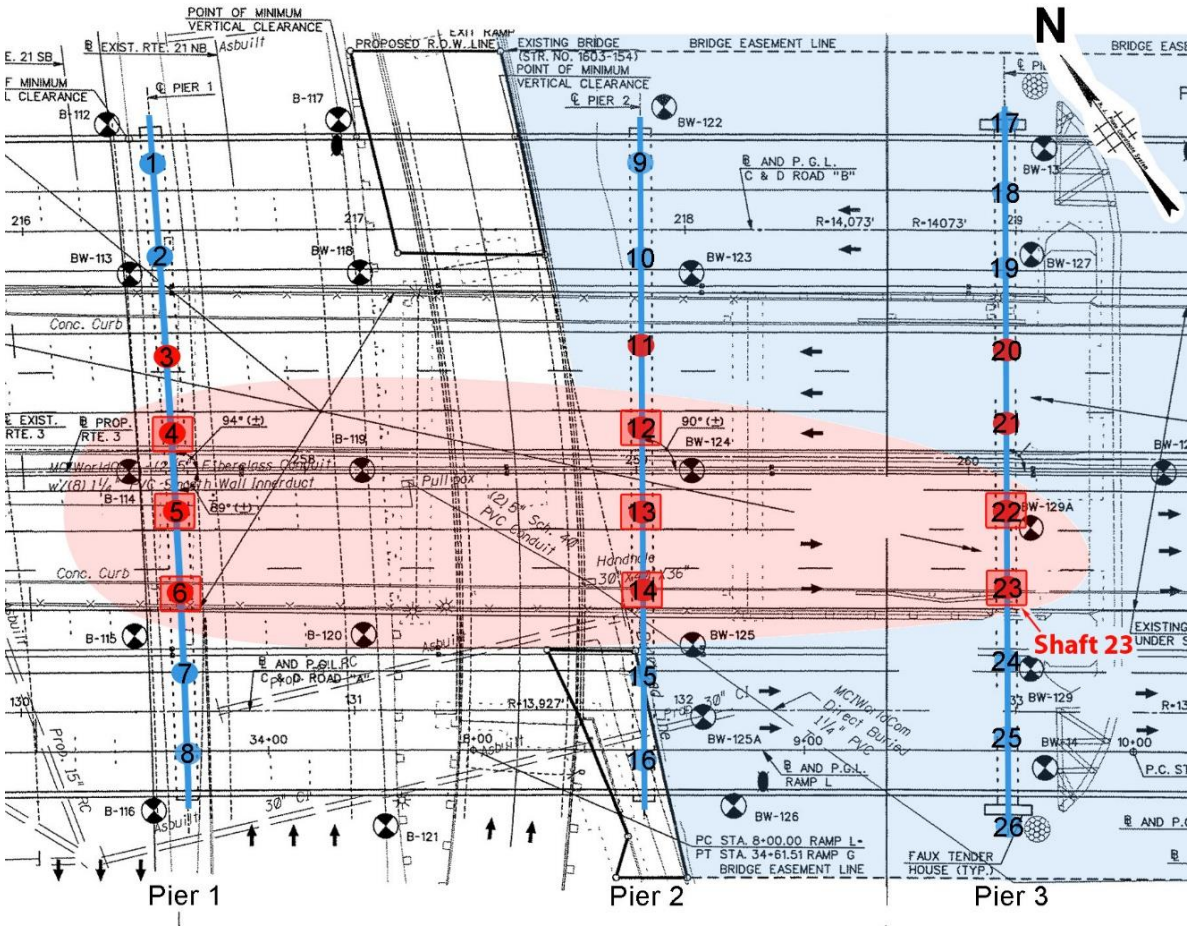

Figure 4 – Site map showing the eight problem shafts (4, 5, 6, 12, 13, 14, 22 and 23 – boxed and numbered red circles) drilled in Piers 1, 2 and 3 and how they define a NW- to SE-trending zone of similar ground effects (pink ellipse) both on land (uncolored) and within the river (blue).

All published references studied describe the Passaic Formation as intact and exhibiting many types of primary and secondary sedimentary structures. Absolutely none of the published research, from over 200 years of study, reported any field- or drill-core based evidence of large openings, voids, caves, or caverns from within the rock formation which is understandable considering the degree of lithification and lack of readily soluble mineral phases that constitute the Passaic rock mass.

Based on pre-bid boring log driller's notes the predominant rock types (82% or 74 of the 90 runs) were identified as consisting of "fresh" and "medium hard" sandstone of red, brown,

red-brown color with minor gray and blue scattered layers. Interlayered "fresh" and "hard" shales of similar coloration account for 18% (16 of the 90 runs). Thus, sandstone predominates over shale in the borings at about a 4.5:1 ratio.

Careful study of the boring data (including a careful statistical analysis of REC % and RQD %), UCS data and geotechnical descriptions indicate that contractors should have anticipated a non-fractured, “medium hard” rock mass of "fair" quality. Based on these and other data, the geotechnical report recommended drilled shafts to rock with deeper sockets for caisson construction and indicated no highly fractured or faulted ground conditions that would require different means and methods than those recommended and employed by the contractor, yet the eel made its way into the bottom of the shaft!

Discovery of the Geologic Cause for a DSC

In order to provide a scientific basis for the as-built contractor experience, we devised and supervised video recordings of a water-filled shaft and a developed a down-hole method of mapping the interior of the 90" (7.5') diameter rock socket extending ~15’ below the 96” problem Shaft #23 in order to generate an associated 2-D map and construct an analog 3-D view of the as-built subsurface geological structure.

In order to calibrate and map the shaft interior we marked the walls by suspending weighted colored ropes with magnetic N, E, S, and W and intervening magnetic compass directions NE, SE, SW, NW so that calibration, recording and calculating the orientation of geological features could be accomplished (Figure 5).

Figure 5 – Various ropes used with weights and C-clamps to hold ropes taught and vertical down the sides of the shaft in order to video each compass rose direction with depth calibration. Analysis of the color-coded videos allowed us to generate an accurate flat 2-D map of the interior of the rock socket.

Careful study of the video was fruitful and allowed for incremental drafting of an accurate 2-D geological map without vertical exaggeration of the 90" (7.5’) Shaft #23 rock socket (Figure 6).

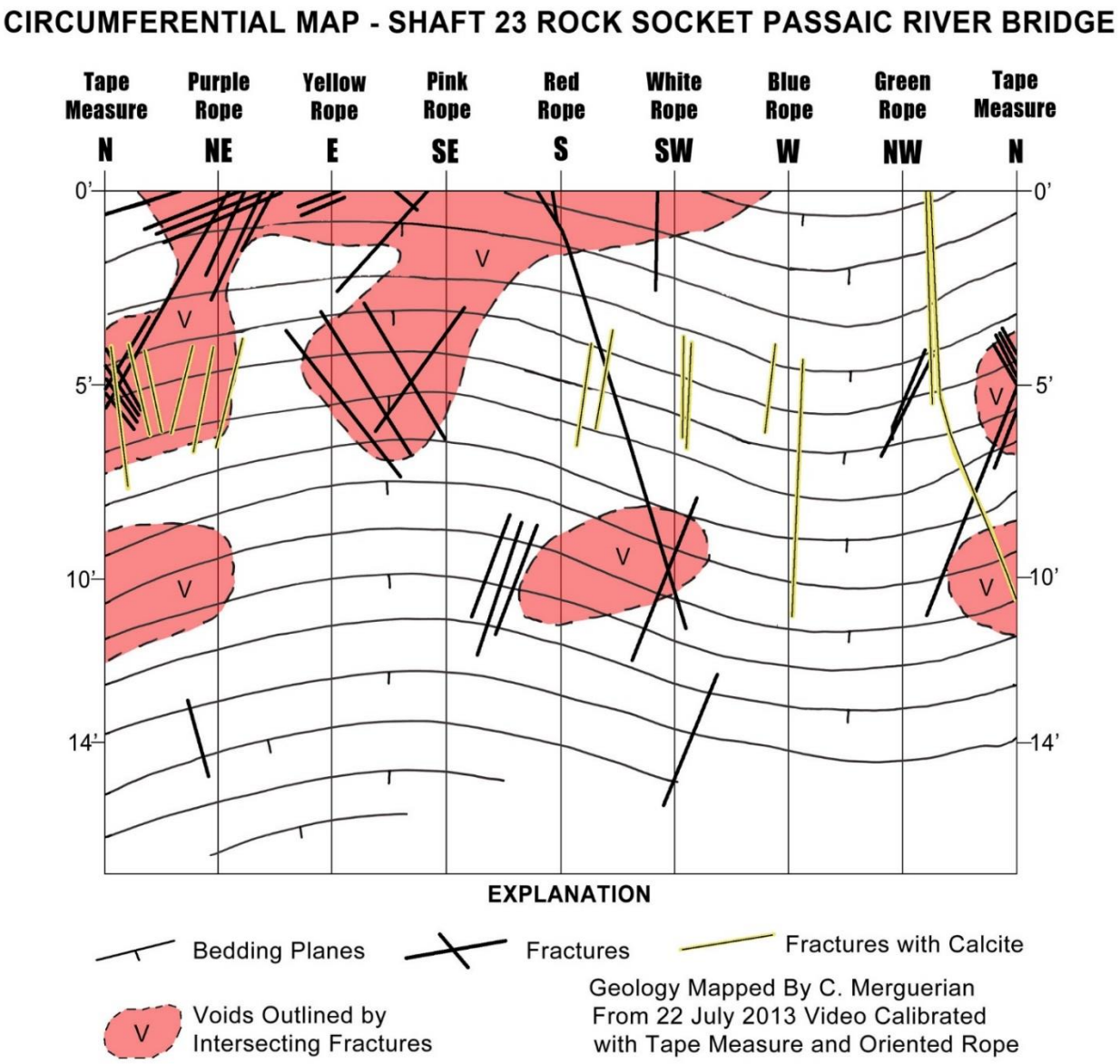

Figure 6 – Circumferential geological map of bridge Shaft #23 rock socket of 90" (7.5') diameter showing orientation of inclined bedding planes (thin black lines with tick marks), intersecting steep to gentle fractures (thick black lines) and open voids where blocks fell out of socket sidewall (v - pink areas). Also shown are mineralized fractures in yellow and black. Drawn with no vertical exaggeration. Compass directions are magnetic.

The compass ropes and depth markings allowed for calculation of fracture orientation using standard aligned compass and three-point methods. It was not until the map was printed onto clear acetate and curled and held together by analog methods into a 3-D cylinder to mimic the ~15' deep rock socket did we recognize the alignment of seemingly separate through-going discontinuities (dark black lines in Figures 6 and 7) and the relationship of the fracture intersections to the mapped visible voids (pink areas in Figures 6 and 7).

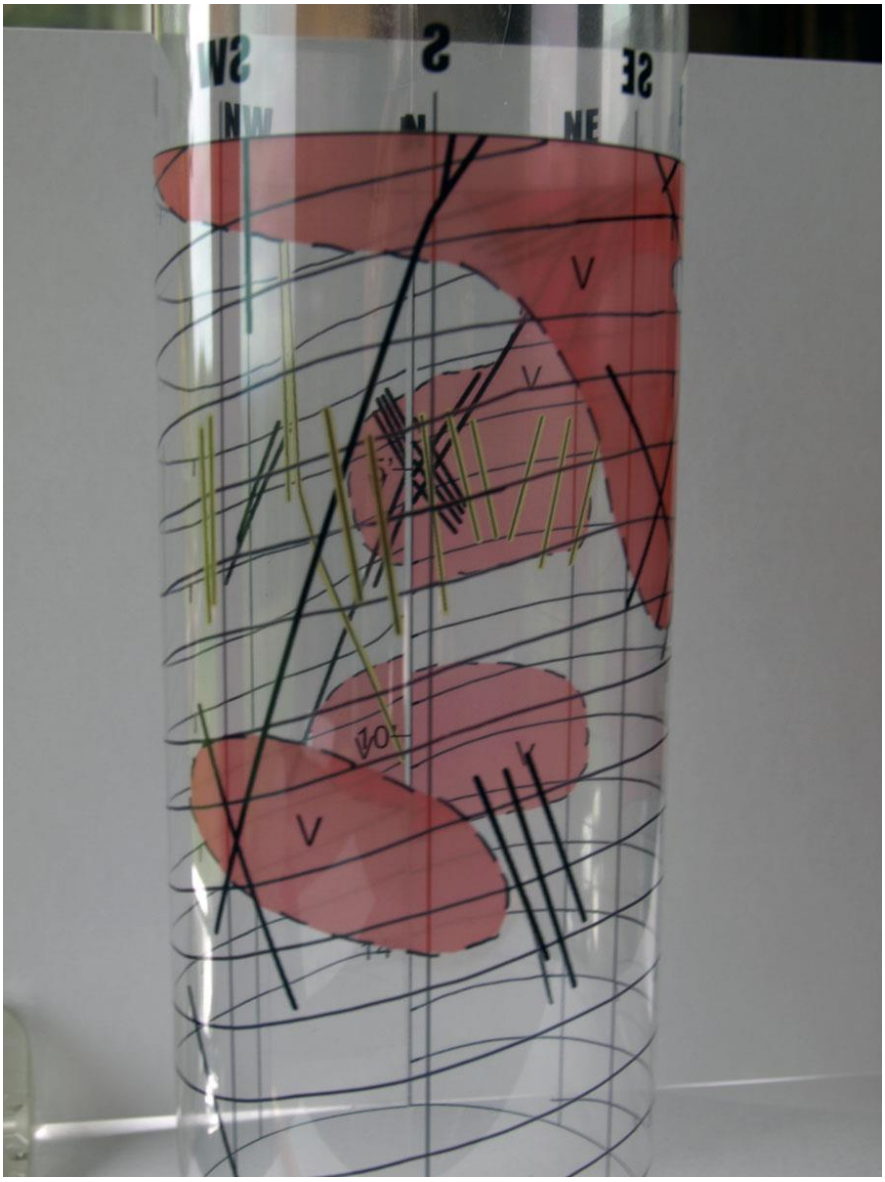

Figure 7 – Northward view of Shaft #23 rock socket acetate map of Figure 6 curled into a cylinder showing the relationship of bedding planes (~14° NW dip [thin closely spaced lines]), NNE-, NE- and NW-trending fractures (steep, black lines), and voids (pinkish areas - v). Note that some of the steeper, NNE-trending fractures (outlined in yellow) are mineralized by calcite or whitish zeolite, common minerals found within faults and joints in the Newarkian strata and also observed in the boulders shown in Figure 3, above. Not obvious are gently inclined (~14°) fractures that parallel bedding near the top of the map at the base of casing.

The steep dislocations fall into three major geometric classes. The most prominent and through-going mapped feature is a fissure that extends through the rock socket center and downward over 10' in extent with a N35°E strike and 75°NW dip (center of image in Figure 7). Also mapped were at least five (5) less extensive fractures that parallel this main fissure as is common in fault zones. There is also a younger set of shorter, closely spaced mineralized conjugate fractures with a N25°E strike and 80°SE dip fanning through vertical to dips of 80°NW. These discontinuities overlap and seem to crosscut the major NE-trending fracture set.

The steeper conjugate fractures sometimes show mineralization with calcite or a whitish zeolite mineral as indicated by yellow and black markings in Figures 6 and 7. A third prominent set of steep fractures strike N40°W and dip 70° toward the NE. A fourth set of dislocations occur near the top of rock. These are closely spaced, shallow in dip and cut bedding at a very low angle. These are simple bedding plane joints that trend NE and dip very gently (~14°) NW.

Figure 6 shows that four major open voids exist in the drilled rock socket of Shaft #23 from the base of the casing to about 8' depth, then again at about 10' depth. The voids are 3' to 8' in extent, extend a few feet deep into the sidewall and are concentrated up-dip in the eastern half-perimeter of the rock socket as would be expected if the blocks initially slid along bedding planes into the rock socket. Many of the open voids were found to terminate against steep planar fracture surfaces suggesting emphatic fault control of blocks that fell into the shaft along the regional dip of bedding planes. Figures 6 and 7 clearly document the relationship between areas of multiply fractured bedrock and associated angular voids detected in the subaqueous videos.

The site inspections, video analysis and mapping performed indicated that open voids and blocky ground conditions experienced at the bridge site by the contractor during rock socket drilling were the result of amplification of geological effects produced by the convergence of natural geological discontinuities (faults and joints). Unfortunately for this bridge construction effort, the gently inclined bedding plane joints intersected by multiple generations of steep to vertical fractures (joints and probable faults) together created blocky ground and difficult construction conditions using standard, tried and true means and methods. All of these related effects (unstable shaft- and socket walls with in-falling blocks of rock and sidewall water- and material-inflows) greatly impeded construction. The pre-bid geotechnical information provided to the bidders did not inform the contractors of such conditions as no mention of faults much less intersecting faults were noted. The unanticipated ground behavior at the eight bridge pier shafts during drilling constitutes a DSC as no one could have reasonably anticipated the effects of such localized highly fractured ground from the provided pre-bid information and other available data.

Note that on Figures 4 and 8 that the eight DSC caissons (Shafts #4, 5, 6, 12, 13, 14, 22 and 23) are not evenly distributed throughout the jobsite but are spatially oriented with a NW to SE alignment parallel to the NW-SE faults. This is additional evidence for a DSC with 17.8% of the 45 shafts affected as the extension of mapped faults conforms to the pink ellipse of affected shafts shown in Figure 8. Thus, there appears to be geological continuity of cause and effect.

Multiple fault and fracture convergence as found at the Shaft #23 site are unusual geometric subsurface conditions. Convergent high-angle fractures superimposed on gently inclined bedding plane joints created blocky ground and the excavation led to voids because of fallout from the sidewalls. The Shaft #23 site showed changed site conditions but the projection of fracture trends to other shaft sites explained the formidable extent of bad ground conditions extending out from the Shaft #23 zone of fracture convergence and intersection.

Subaqueous Bridge Shafts Summary

The investigation of rock conditions in scientific support of a DSC claim in connection with this subaqueous bridge shaft drilling program included site inspections, geotechnical report

analysis and map-based geological analysis. This investigation documented open voids and unstable sidewall conditions at Shaft #23 and determined a natural geological cause for the DSC. Anomalies at Shaft #23 extended northwestward to include other shaft sites where similar voids and blocky, unstable ground resulted in excessive water- and material-inflows and shaft sidewall blocky fallout. (Compare Figures 6 through 8.) suggesting far-ranging fault effects of the N40°W-trending fault set that dips ~70°NE.

These hitherto unknown natural subsurface geological conditions impeded construction using industry standard means and methods and were the basis for successful DSC claims by an experienced contractor as no one could have reasonably anticipated such rock mass conditions (convergent faults at Shaft #23) from the documents provided pre-bid nor from the existing scientific literature.

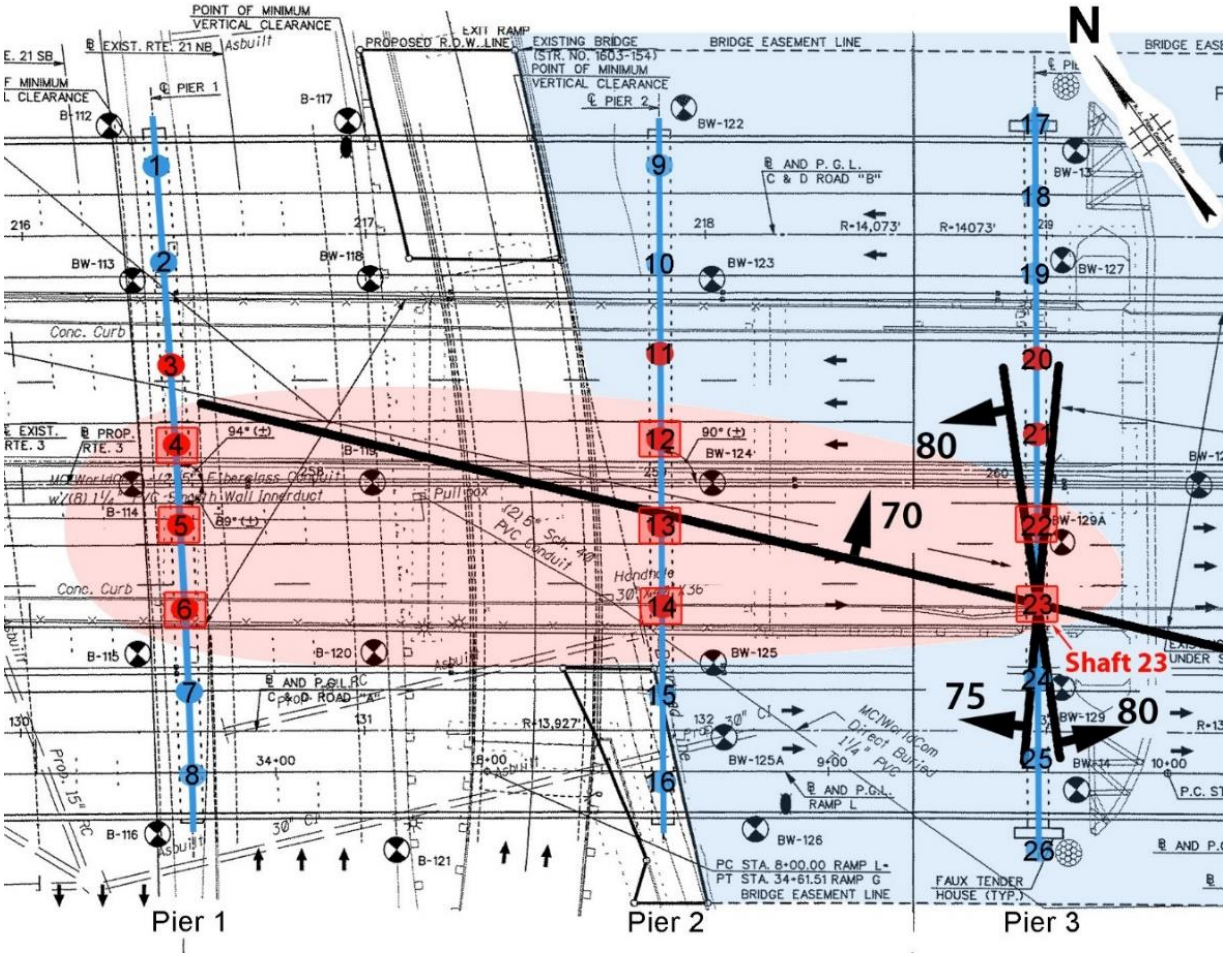

Figure 8 – Plan view of DSC claim area (pink ellipse) that includes the eight problem shafts encountered during Piers 1, 2 and 3 drilling of the bridge. The faults and related joints mapped from Shaft #23 are plotted to show their crosscutting relationships and geometric structural control on the associated problem shafts of the DSC claim. Note that the three steep fracture systems shown in Figures 6 and 7 (N40°W strike, 70°NE dip; N35°E strike, 75°NW dip and N25°E strike with conjugate dips fanning from 80°NW through vertical to 80°SW). These intersecting fractures extend outward from that zone of convergent intersection and cut gently inclined in-situ bedding planes and sub-parallel shallow joints at Shaft #23. Note that all faults were plotted with respect to True North as the magnetic declination at the site in 2013 was -12° 50' (12° 50'W of True North).

Terrestrial Caissons

The second geotechnical vignette we share here involves unanticipated ground conditions encountered during down-the-hole hammer drilling for installation of multiple caissons for a high-load above-ground NYC construct. This site is underlain by ~100' of Holocene fill and Pleistocene strata and basal gently inclined Cambro-Ordovician rocks of the Inwood Marble Formation. Production drilling for forty-four (44) or 30% of the 148 installed caissons experienced anomalous groundwater and/or sediment inflows and associated ground effects during construction, well beyond any reasonable anticipation of risk. Both at the base of the overburden and while drilling rock sockets notable outpourings of water + material included spectacular instances of geysering (Figure 9), transforming this NYC construction site into a *"Disney water theme park"*. Below we discuss the persistent ground effects experienced during production drilling and our use of a three-point fracture plane solutions, geological maps and sections to depict the natural bedrock condition detected beneath the site that led to a DSC claim.

Figure 9 – View of as-built anomalous water + material flow and geysering associated with caisson drilling in November 2015 at a terrestrial caisson/pile drilling job site. (Contractor image.)

The DSC claim pursued by the contractors was based on unanticipated high transmissivity and communication at the base of the overburden and within the upper part of the marble bedrock layer. This introduced water and material into many caissons and rock sockets which could not have been anticipated by the contractor based on the geologic data supplied in the pre-bid documents nor in the provided boring logs. After costly excessive water mitigations on site in 2015 through 2016 we were able to examine the soil and rock core samples in early 2017 to aid in our geotechnical analysis.

The scientific conclusions of our support efforts rely partly on a basic three-point solution analysis of like features noted in the pre-bid logs and our prior experience elsewhere in the same formation. Here we detected through-going, gently-inclined open water-bearing fracture zones dipping beneath the job site that produced an unknown subsurface *"plumbing system"* which fed the excessive water and sediment flows encountered during subsurface drilling. Extraction and redistribution of subsurface water and sediment not only hindered the construction effort but created serious ground effects (anomalous surface flow volumes, ground cracks, cratering, boils and local building settlement and cracking).

The stratigraphy of roughly 100’ of overburden from the top down included Holocene fill, Pleistocene sand units, intervening varved strata and basal till below which penetrations into the Inwood Marble bedrock were met with persistent excessive water and material inflows (Figure 10).

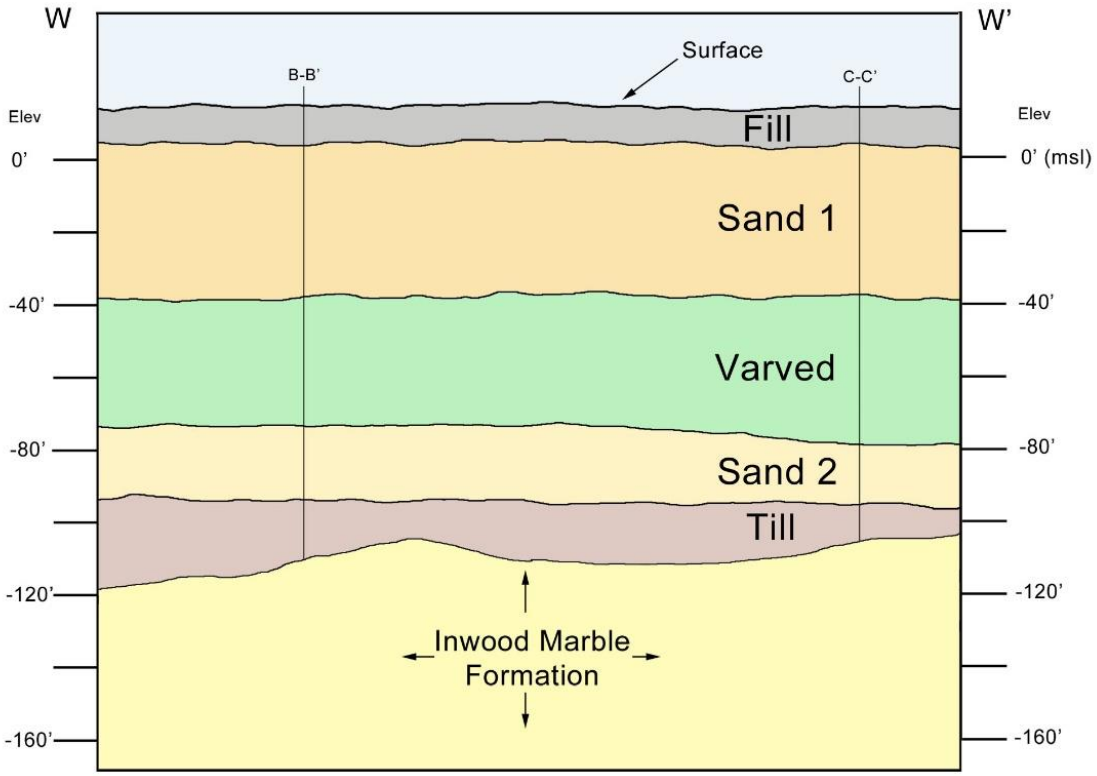

Figure 10 – Across site roughly W-E geological profile section drawn from data supplied in the geotechnical report showing overburden strata and the buried Inwood Marble bedrock layer. This view of the site was the anticipation and design criteria for the contractor’s approved means and methods.

The problem caisson sites were <u>not</u> scattered throughout the site footprint which argued against any notion of improper means and methods (down-the-hole hammer systems) which were approved by the owners. Rather, the problem caissons were clustered in the northeastern corner of the site (Figure 11) where an adjacent, unsupported old-construction brick and mortar building settled, tilted, cracked and became severely damaged. What is more, water and material communication occurred between widely separated drilled caisson/pile sites indicating significant subsurface connectivity of transmissive features. Site reports by the contractors and the owner's resident engineers reported *"heavy water, sand, and rock; excessive water from casing; thick (heavy) sediment inflows up to 25'; seams; rock ledges; dirty discharge; large rocks; sockets making water; communication between open drill sites; flooding of the jobsite; spoils on the ground; and equipment damage including broken shoes, rig tilting, hammer clogging and unanticipated hammer firing."*

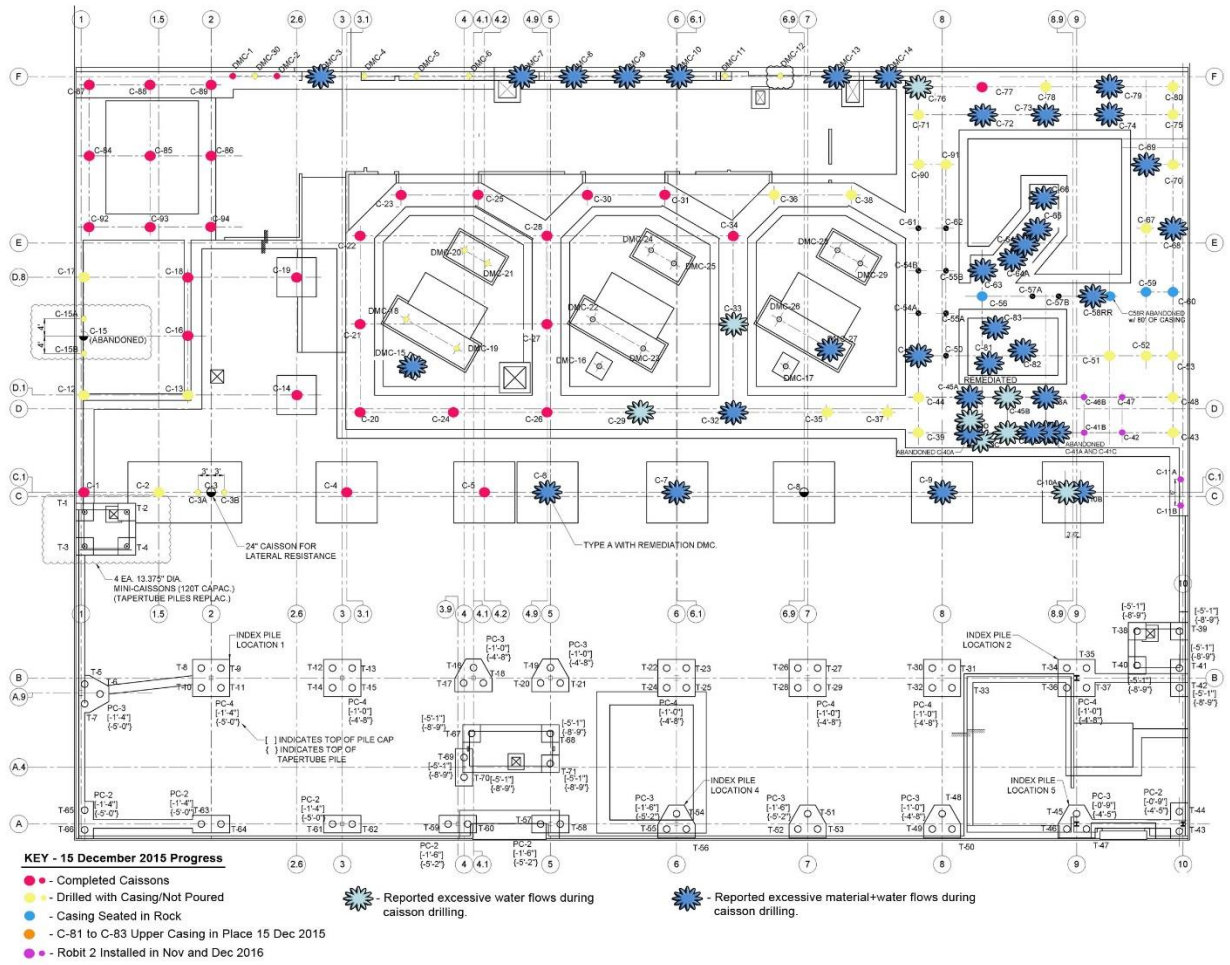

Figure 11 – Site plan showing the clustering of forty-four (44) caisson sites where installation was met with construction difficulties associated with flowing water only (light blue symbols) and water + material outflows (dark blue symbols). The remaining caisson sites shown in red, yellow, orange, black, noncolored and purple were drilled without difficulty. Project north to top of map.

Borings and Boring Log Analysis

In order to better understand the pre-bid anticipation vs. the as-built contractor experience, we performed a careful study of the geotechnical information provided by two geotechnical reports and 17 associated boring logs. Figure 12 shows the positions of the 17 pre-bid borings performed in 2007 and 2013 and whose logs were included with the geotechnical reports. These data were used by contractors to evaluate the subsurface conditions and formulate baseline parameters for their winning bid and the means and methods for the construction project. Little data on foliation or compositional layering was to be found in the boring logs but the orientation of foliation joints show gentle dips (0° to 30°) for many of these primary features.

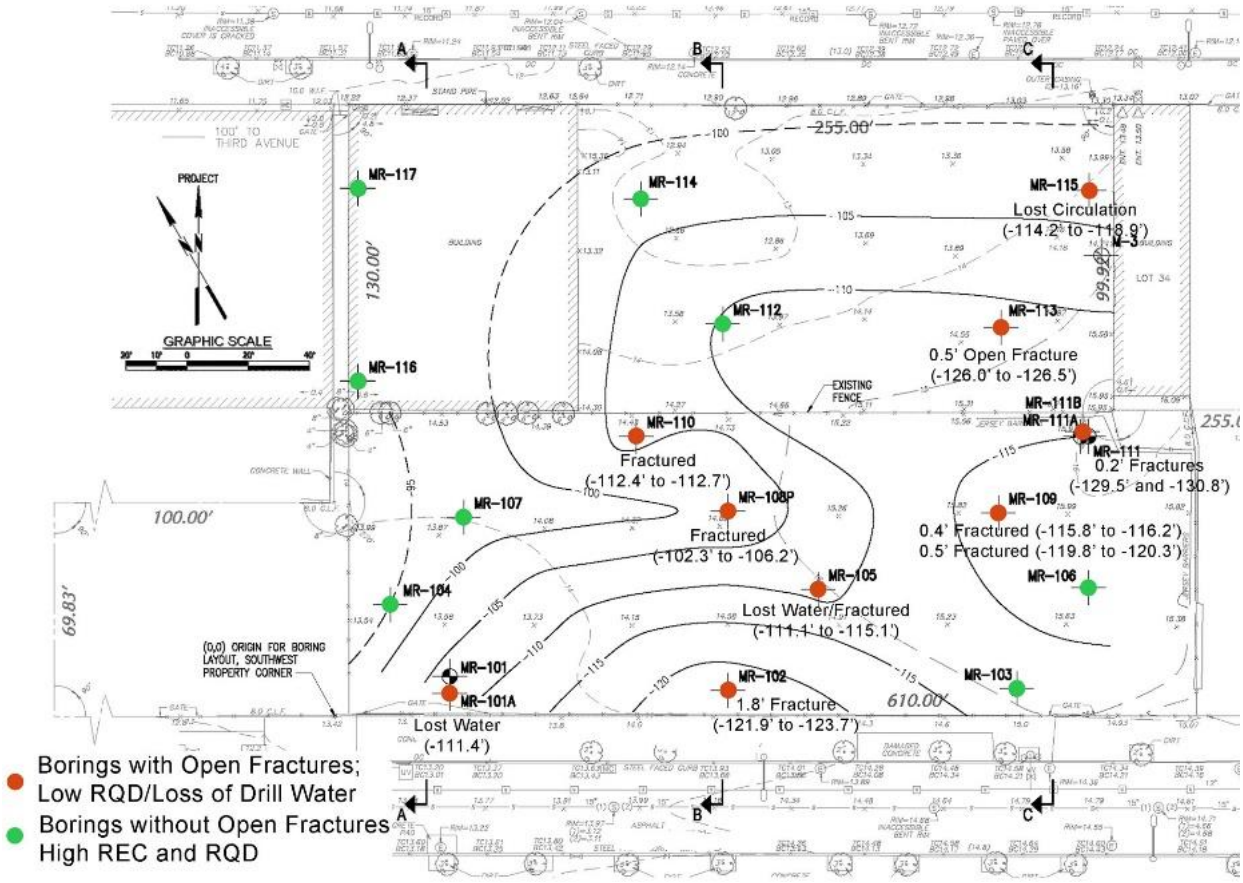

Figure 12 – Site plan map showing topographic data, annotated boring locations (MR-series) and top of rock contours within the footprint of the site. Nine borings with open fractures, low recovery and RQD values, and/or reported *"loss of drill water"* are shown in red. Eight competent borings without reported open fractures and with high recovery and RQD values are shown in green. Note the E-W clustered trend of the red borings.

Examining the soil and core samples in February 2017confirmed that no contractor could have anticipated the true ground conditions. Visual inspection showed that the core was competent and tended to be massive with some jointing. Thus, a pre-bid core analysis by any contractor bidding for work and guided by the supplied information on REC and RQD % would create an anticipation of hard- to medium-hard, blocky to closely jointed marble but would

provide no hint as to the lateral extent, connectivity, nor potential for hydrologic transmissivity of any fractures within the marble rock mass.

Rather, the as-built experience involved cross-hole communication, excessive water inflows, sediment flows, ground settling, ground cracks and cratering at caisson drill sites indicating hidden difficulties within the rock mass. Our as-built analysis indicated that the subsurface fracturing is not sporadic but defined at least one and probably two gently inclined open aperture fractures that varied from thin seams to fracture zones possibly up to 4.7' thick both near and below the top of rock. Both fractures intercept the top of rock, are separated by about 10' of solid rock and dip about 1° (upper fracture) and 5° (lower fracture) eastward beneath the site. Careful study of down-hole inspection videos showed the open fractures despite their blurry subaqueous murky setting yet the owner and their representatives would not accept our results and a lengthy and contentious battle took place that was just recently settled by mediation in 2021.

Three-Point Fracture Plane Solutions

Once boring logs were converted from depths to elevations comparable features detected in the logs allowed us to group borings showing similar traits. This allowed for application of a simple tried and true mining visualization technique (the three-point problem solution) to identify strike and dip of a planar feature given three points of varying depth and known geographic position. The technique assumes uniformity of strike and dip and planarity of the feature which are reasonable assumptions given the small footprint of the site – about a half a city block. The technique is a graphical/trigonometric one that involves identification of a maximum, minimum and intermediate elevation of a planar feature such as a mineralized ore vein or through-going fault or fracture (Donn and Shimer 1958). By drawing a triangle that encloses the surface position of sets of three boreholes, as depicted in Figure 13, a unique point on the line that joins the maximum and minimum elevation values can be scaled that equals the intermediate elevation. A line joining this scaled point to the intermediate boring shows, by definition, a line of equal elevation (strike or trend) of the planar feature. Calculation of dip is straightforward once the strike and the variation of high and low pierce points are identified using standard orthographic projection fold-line techniques.

The clue that drew our attention came in the form of three widely separated borings that reported *"loss of drill water"* (MR-101A, MR-105, and MR-115). Loss of drill water and/or drop in the drill stem below top of rock is usually an indication of open voids or fractures. MR-101A lost drill water at -111.4' elev., MR-105 lost drill water between -111.1' and 115.1' elev. (a 4.0' interval), and MR-115 lost drill water between -114.2' and -118.9' elev. (a 4.7' interval). Since no casing is used in driving NX-core, drill water can escape the borehole at the initial pierce point of a void or fracture despite the report of lost drill water over a 4.0' (MR-105) to 4.7' (MR-115) interval. As such, these values can be considered <u>maximum</u> width values for these features. Alternatively, the void or fracture may encompass the entire interval. In order to perform the three-point analysis we employed an average *"loss of drill water"* elevation value for MR-105 (-113.1' elev.) and MR-115 (-116.6' elev.).

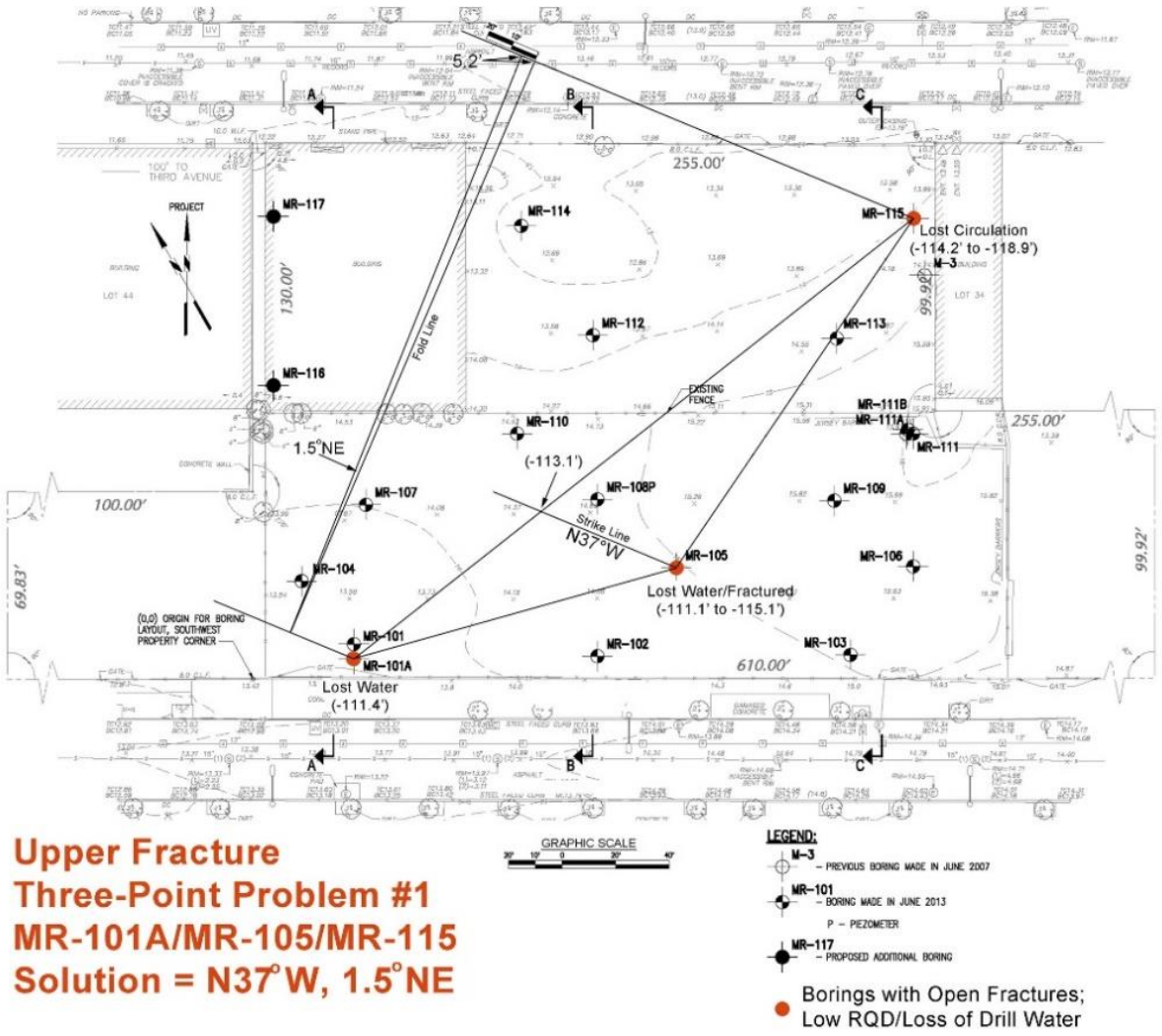

Figure 13 – Three-point solution #1 for upper fracture using data from borings MR-101A, MR-105, and MR-115.

Using the method described above the three-point problem solution #1) shows that three *"loss of drill water"* borings provided a solution that identifies an open fracture or fracture zone oriented N37°W, 1.5°NE. In order to test for and verify the lateral extent of the feature detected in Figure 13 we also grouped boring MR-101A, MR-105, and MR-115 as similar because of an RQD drop in Run 3C (64%) after much higher values in Runs 1C, 2C and 4C (REC and RQD % values both ranged from 95%-100% in these runs) and the presence of open (0.3') fractures. This allowed for two additional three-point solutions using MR-101A, MR-105, and MR-110 [Solution #2 = N12°E, 1°SE] and MR-105, MR-110, and MR-115 [Solution #3 = N3°W, 1.5°NE] (not shown here) which not only overlapped with Figure 13 result but yielded nearly identical strike and dip solutions.

Keeping in mind that strike varies greatly for very gently inclined features and is, in fact, infinite as one approaches 0° dip, all three solutions were considered to be in agreement - they defined an open, through-going continuous upper fracture zone from one end of the site to the

other with an approximate N-S strike and an average essentially subhorizontal eastward dip of 1.4°. Clearly, three separate groups of overlapping solutions that yield nearly identical orientations that support the existence of the subsurface feature. In addition, the solutions provide continuity for identifying the lateral extent of the fractures below the site as discussed in a later section.

Borings MR-102, MR-111, and MR-113 show similar traits as those above in that they indicate a marked decrease of REC % and RQD % in lower core runs below a reach of competent rock. Using these data, three-point problem solution #4 shows a secondary deeper (lower) open fracture oriented N52°E and dipping 5°SE (Figure 14). The lower fracture is not as wide (0.2' to 1.8' wide) as the upper fracture and occurs 10' to 14' deeper than the upper fracture with slightly steeper dip.

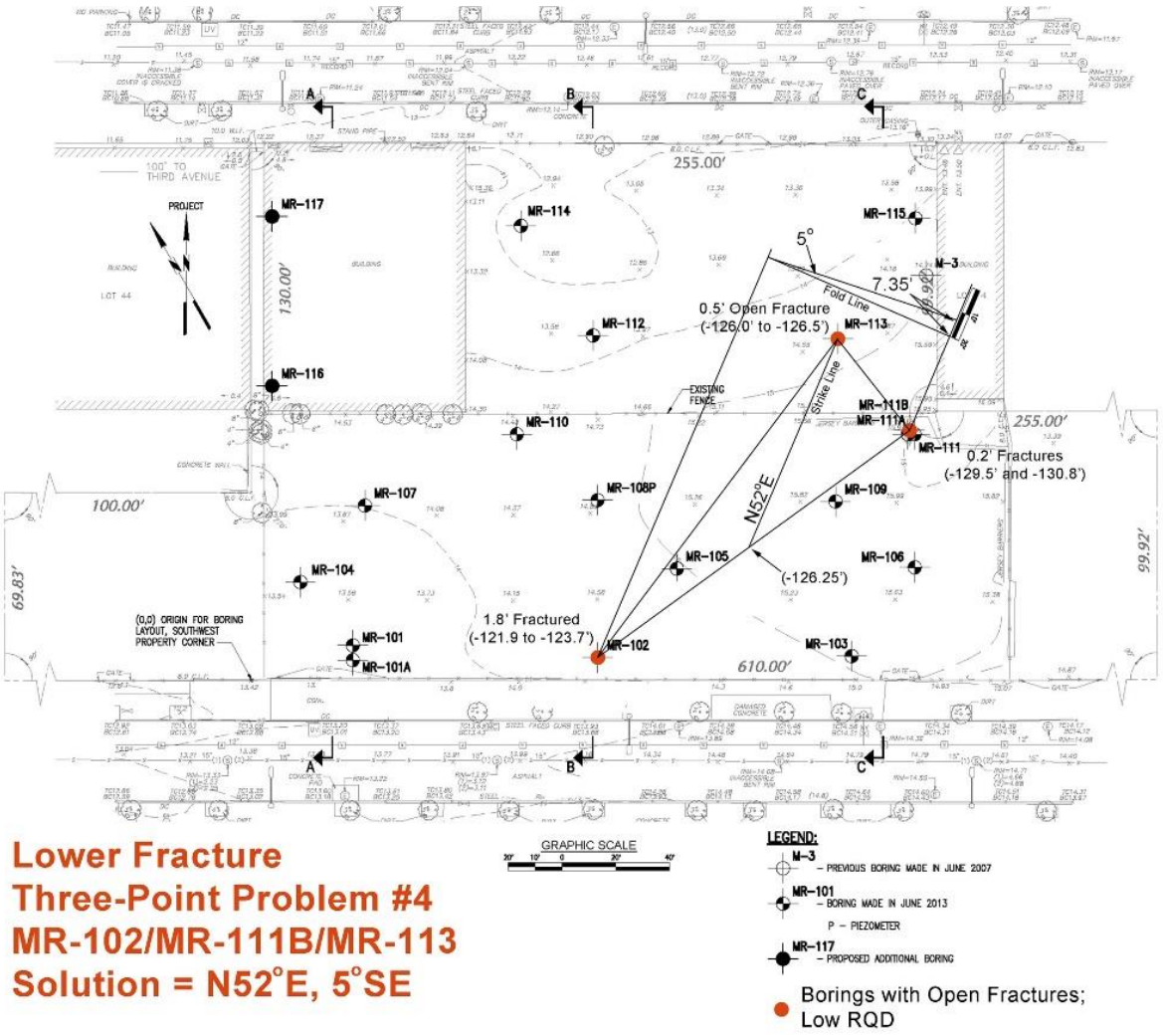

Figure 14 – Three-point solution #4 for lower fracture using borings MR-102, MR-111B, and MR-113.

Thus, the three-point solutions identified two horizons of open aperture fractures that descend across and below the site and dipping gently eastward within the marble rock mass. Clearly, they are important players in the subsurface plumbing system that underlies the site.

Geology of the Inwood Marble Formation

Another pertinent aspect of the subsurface geology lies in the rock type variations that constitute the Inwood Marble Formation of NYC. The project site is covered by roughly 100' of overburden and then underlain by the venerable Inwood Marble Formation, originally named by Merrill et al (1902). Formed from metamorphosed lower Paleozoic (~550 Ma) former shallow water marine carbonate and intercalated clastic sediment, the Inwood Marble Formation now consists of well-layered, typically massive dolomitic marble, subordinate calcite marble and minor calc-schist. Constituting a folded layer over 700' thick in NYC, it underlies the Inwood section of northern Manhattan (type locality), the Harlem lowland NE of Central Park, occurs as thin belts in the East River channel, in the subsurface of southeastern Manhattan and also crops out in the Bronx and Westchester County (Merguerian, Merguerian and Cherukupalli 2011).

But the devil they say, is in the details. By contrast to the **dolomitic** marble that constitutes the bulk of the Inwood Marble Formation in NYC a coarse-textured **calcite** marble is found near the top of the formation where it is interlayered with the overlying Walloomsac member of the Manhattan Schist (Merguerian 2008a, b). The same sub-unit was also found to underlie this site, based on rock samples collected during rock socket drilling and mucking operations. This unit, because it is a very coarse-textured pure calcite marble (+/- diopside and phlogopitic mica) rather than the typical dolomitic marble of the Inwood, it is susceptible to dissolution and disintegration along crystal boundaries and internal fractures by cold groundwater over time. Calcite ($CaCO_3$) is simply more soluble than dolomite ($[Ca+Mg]CO_3$) in cold fresh water resulting in dissolution over time by circulating groundwater. As such, this distinctive marble sub-unit unit is particularly prone to disintegration and weathering issues potentially resulting in subsurface water transmissivity.

We have mapped the coarse-textured white calcite marble sub-unit at the top of the Inwood Marble Formation at the top of rock at a contemporary project a block from this site and elsewhere in NYC (Isham Park, Inwood Park, and at a utility tunnel and associated large-diameter shaft site in the Bronx). What is more, our February 2017 examination of the drill core and HCl acid testing of all of the core runs showed that the upper run (1C) of many of the borings (10 out of 17 runs or 59%) exposed calcite marble at the top of the run or in cored boulders resting above the top of rock (MR-102, -103, -104, -106, -109, -110, -111B, -112, -114, and -115). The hint of the gentle inclination of the compositional layering (bedding) in this area allows for the interpretation that much of the "white marble" described in the logs at or near the top of rock is the same white calcite marble which can harbor open-aperture fractures and provide channels and conduits for water (+/- sediment) transmission. The fact that calcite marble did not **always** result in difficulties indicates that the calcite marble is **not always** prone to disintegration. As we found in 2009 where we mapped a deep drill and blast large-diameter shaft site in the Bronx with similar overburden depth, calcite marble can be disintegrated and water-bearing where it is cut by natural structural fractures in the rock mass that allowed groundwater interaction with the calcite marble to dissolve, crumble and open over time.

Unanticipated Bedrock Conditions

The top of rock in NYC is hydrologically active. Research performed by the U.S. Geological Survey in cooperation with the NYC DEP has shown that groundwater recharge in Manhattan takes place via percolation of meteoric water into NYC parks, especially Central Park (Stumm et al. 2001a, 2001b, 2004 and 2007) and is distributed away from the exposed bedrock knolls of central Manhattan radially outward. From there it permeates the soil (regolith) and also flows along the top of rock and into any existing bedrock conduits. Transmissive bedrock flow is often facilitated by low-angle to horizontal open aperture fractures found throughout the crystalline bedrock of NYC but especially in the soluble calcitic sub-units of the Inwood Marble Formation as discovered at the aforementioned shaft site in the Bronx (Stumm et al. 2013).

Two very gently inclined fracture zones descend below the top of rock at the job site based on the four fault plane solutions presented above. Figure 15 shows a conservative visualization of the east-dipping subsurface fracture system footprint (truncated blue ellipsoid) and shows a rather remarkable spatial coincidence with borings whose logs reported water loss during drilling and logs showing fractures below more competent rock. The extended blue arrows with blue question marks are a reminder that the fractures certainly extend for some distance along their strike and dip and may extend well beyond the zones shown in blue.

Line of section W-W' depicts a vertical profile section of the hitherto unknown subsurface condition (Figure 16). The section was drawn using data provided by the geotechnical report, including the core logs, topographic map, depth to bedrock map and soil profiles and our three-point analyses. The upper fracture varies in width up to a potential maximum of 4.7' and slopes ~1° eastward across the site between -111' to -116' (elev.). The lower fracture slopes from -121' to -129' (elev.) southeasterly at 5° based on one fault plane solution (See Figure 14.) and strikes N52°E but shows similar traits. It appears to dip at 2° in the line of section (W-W' in Figure 16) since it would depict an apparent dip given the non-orthogonal angle between the strike and chosen line of section. The strike for the upper fracture, as determined from the three-point problem solutions ranges from N37°W to N12°E and thus averages roughly N-S as shown by the blue strike lines in Figure 15. Clearly, the strike orientation of the lower fracture is not as well constrained given the solitary solution however we did not question its existence.

The profile section of Figure 16 shows that the upper fracture zone intercepts the buried top of rock near borings MR-101A and MR-102. It intercepts and connects directly with the till unit of the regolith. Here, at the western corner of the site where top of rock slopes down, the lower fracture will also intercept the top of rock, but off-site.

Thus, **both fracture zones** intercept the top of rock and connect to water-saturated regolith toward the west and as such provides a conduit for significant lateral flow of groundwater and sediment within the bedrock. Based on the data near MR-111B and MR-113, the upper fracture zone is at or near the fractured top of rock as shown diagrammatically by the pink elliptical zone in both map and profile section. (Compare Figures 15 and 16.) This hydrologic connection, even without any steep fractures, creates a unique plumbing system

below the site with multiple direct connections between open water-bearing fractures from 0.2' to 4.7' in width and the permeable water-saturated regolith (water table ~+0.7' elev.).

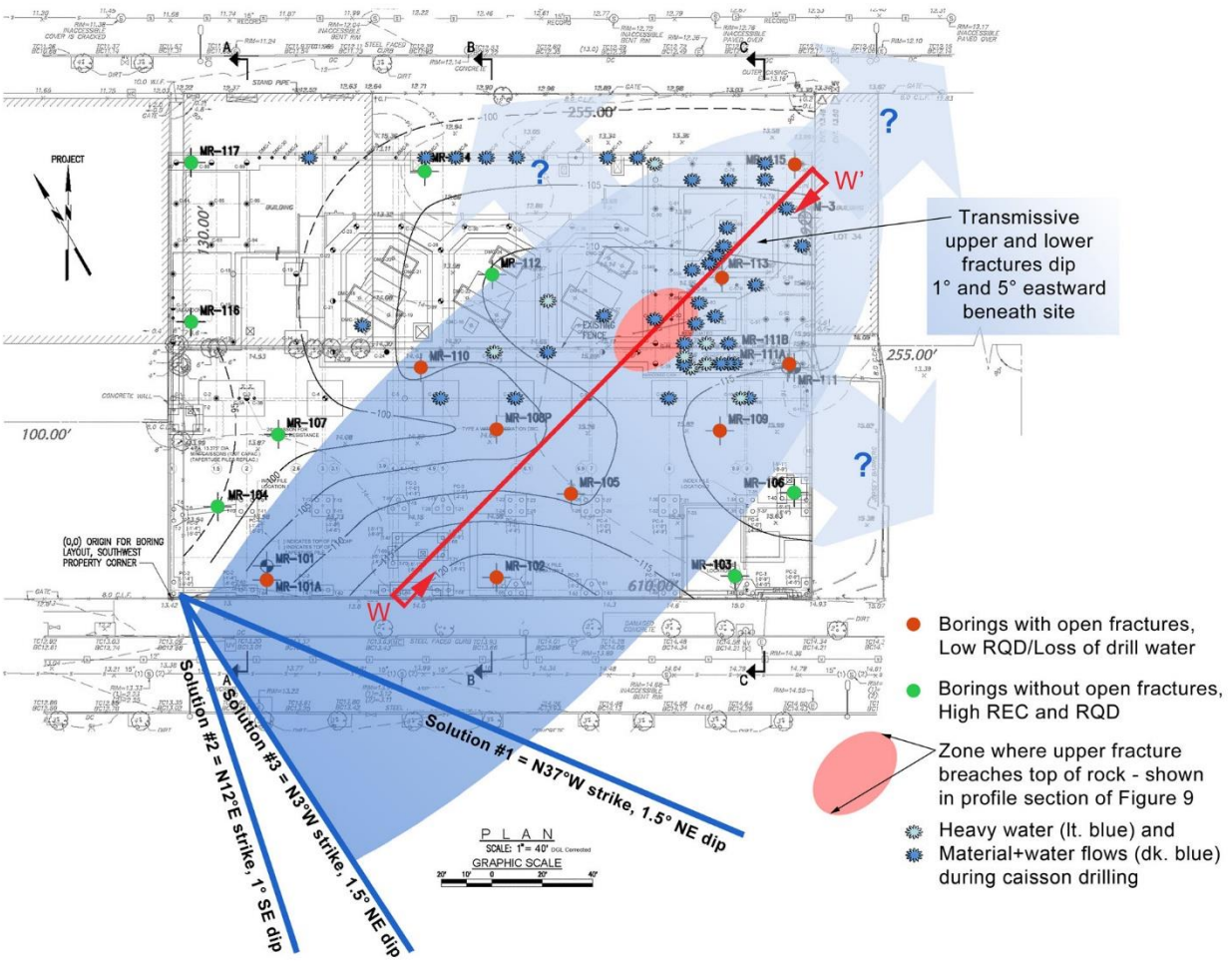

Figure 15 – Simplified plan map showing the three strike solution results of the three-point analyses presented in Figure 13 and 14 (dark blue lines) and two additional solutions not shown and borings harboring open fractures, low REC/RQD % and reported loss of drill water (red dots). Note the spatial coincidence of these borings with the projected footprint of the transmissive upper and lower fracture zones (eastward dipping blue ellipsoid) and their possible extensions down-dip and along strike (extended blue arrows). Also projected upward into plan view is the breached zone shown below in Figure 16 where the upper fracture zone is at or near the top of rock (pink ellipse).

A comparison of Figures 11, 12 and 15 shows very clearly the remarkable spatial correlation between the forty-four (44) caissons where drilling reports indicated deep water-related drilling issues (blue stars in Figure 11), borings with open fractures and/or low REC %/RQD % (red dots in Figure 12), the zone where the upper fracture is at or near the top of rock and the eastward dip and projected potential lateral flow extensions of the subsurface upper and lower fractures (pink ellipse, truncated blue ellipsoid and blue arrows in Figure 15). What is more, the fractures intercept the overburden (See Figure 16.) and provide a unique plumbing system that apparently effected local hydrologic equilibrium when disturbed by drilling. Absent a detailed analysis as presented herein, the pre-bid information was simply inadequate to identify

these deep geological features, their connectivity to the overburden, or to predict the drilling-related adverse effects.

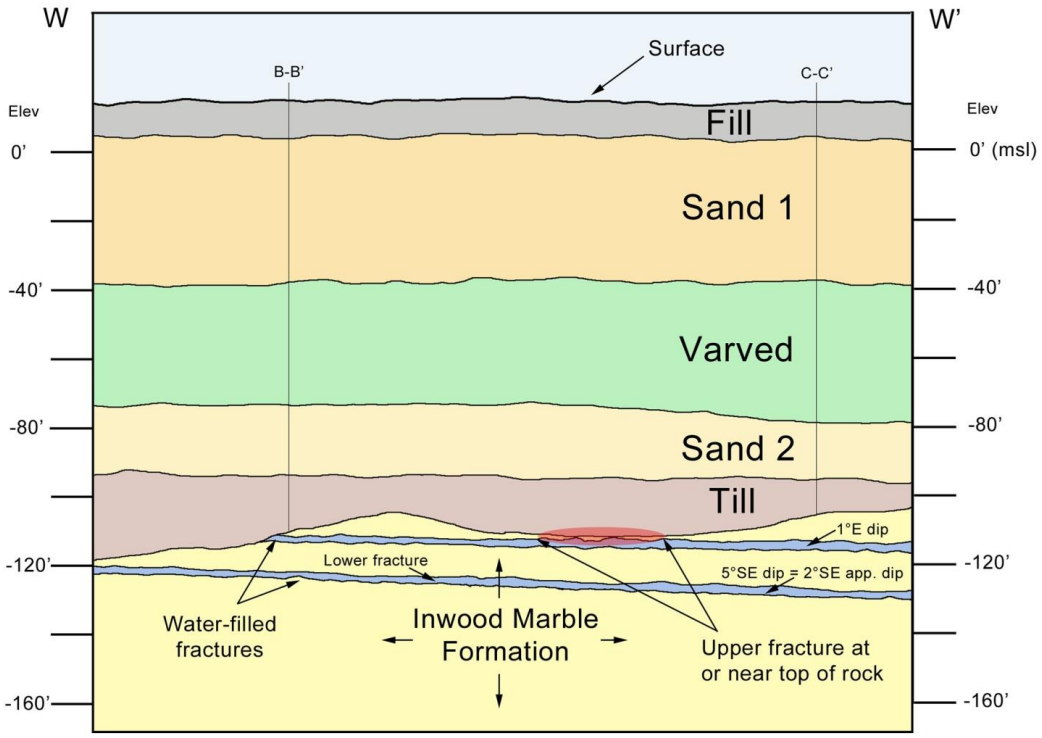

Figure 16 – Roughly west to east profile section (W-W') keyed to Figure 15 showing overburden strata and Inwood Marble bedrock containing water-filled fracture zones (blue) detected beneath site using three-point problem solutions. Section is drawn roughly perpendicular to N-S strike of bedrock fractures. Water-filled transmissive bedrock fractures from three-point solutions are based on my interpretation of data from boring logs and by using the top of rock contour map and geological sections provided by the pre-bid geotechnical report for control. Note the unique bedrock to overburden plumbing system provided by the open-aperture subsurface fracture zones that intercept the top of rock in a few places. (Drafted without vertical exaggeration.)

Terrestrial Caissons Summary

This geotechnical investigation and associated maps and diagrams have shown that very gently inclined through-going upper and lower bedrock fractures provided open, laterally persistent subsurface conduits for fluids within the otherwise competent Inwood Marble rock mass. This has resulted in anomalous water and material transport particularly where the water-charged fractures were penetrated by construction drilling efforts. The provided three-point fracture plane solutions allow for visualization of the two very gently inclined open fractures that dip eastward from 1° to 5° at two different depth ranges separated by about 10' of dominantly competent hard- to medium hard marble rock with high REC and RQD % values.

The differing site condition concept in lowest bid contracts allows for calculation of bids without adding increases for risk contingency. The purpose is to level the playing field and to make contractors whole when unforeseen ground conditions present themselves. We, using geological techniques, showed that the combined effect of open-aperture fissures in bedrock

dipping beneath the site provided a unique plumbing system that allowed for hydrologic connectivity and localized communication between the drilled caisson sites, the water-saturated till (T) and confined lower sand layer (Sand 2) and the bedrock (R). This geological condition resulted in ground effects that impeded construction. As such, this can only be considered a DSC since no mention of this anomalous natural geological condition was described in the pre-bid documents.

No contractor would be able to perform such an analysis as presented above nor retain an expert to arrive at this result pre-bid nor would such an analysis be expected based on the geotechnical information provided. (Compare Figure 10 [anticipated] and 16 [as-built].) Our opinion at the time of this consult was that if a geological expert with intimate knowledge of the as-built experience and the regional geology were able to evaluate the pre-bid core and core logs he or she may have been able to provide a "retrospective explanation" to explain the actual ground conditions (as we have done in this segment) but no one could have predicted or anticipated the true ground condition pre-bid nor its effects on construction costs based on the supplied geotechnical information - a hallmark of a valid DSC claim.

TBM Tunnels

The third construct we would like to highlight took place in the late 1990s and was a roughly 5-mile-long, 23'2" diameter water tunnel bored by a Robbins hard-rock single beam TBM – the most powerful TBM ever built and utilized at the time (Figure 17).

Costly by their very nature and occurring in an unforgiving subsurface environment, tunnel drives in hard rock crystalline terrains require careful geotechnical analysis. DSC claims in such efforts are significant in scope and cost. Our work in tunnels spans four decades and from these efforts we choose one to discuss. We refer you to four papers concerning geological controls on effective hard rock TBM tunneling in crystalline terrains that delve further into the details and parameters of tunneling in NYC strata (Merguerian 1994, 2005a, 2005b, 2008). For reasons of confidentiality, we will identify the tunnel by number - herein named Tunnel #1.

The main issues encountered on this job were much lower than anticipated TBM advance rates, side-wall and crown instability, invert heave, short-stand up times and resulting missed construction deadlines and lost production costs. The main culprits in this case were the Geotechnical Baseline Report (GBR), a contract document which identified the wrong NYC rock formation (Hartland Formation) with rock mass properties vastly different from that which was encountered and a pre-bid drilling program that was too widely spaced and under-analyzed. This consulting engagement required a number of parallel geological efforts rooted in detailed mapping of the entire tunnel, petrographic analysis of collected rock specimens, rock mass statistical analysis which included lithotypes, mineralogical and density studies, geochemical and geochronologic analysis, characterization of zones of geological anomalies and comparisons of decreased advance rates and utilization to geology and as-built TBM performance data (Merguerian and Ozdemir 2003).

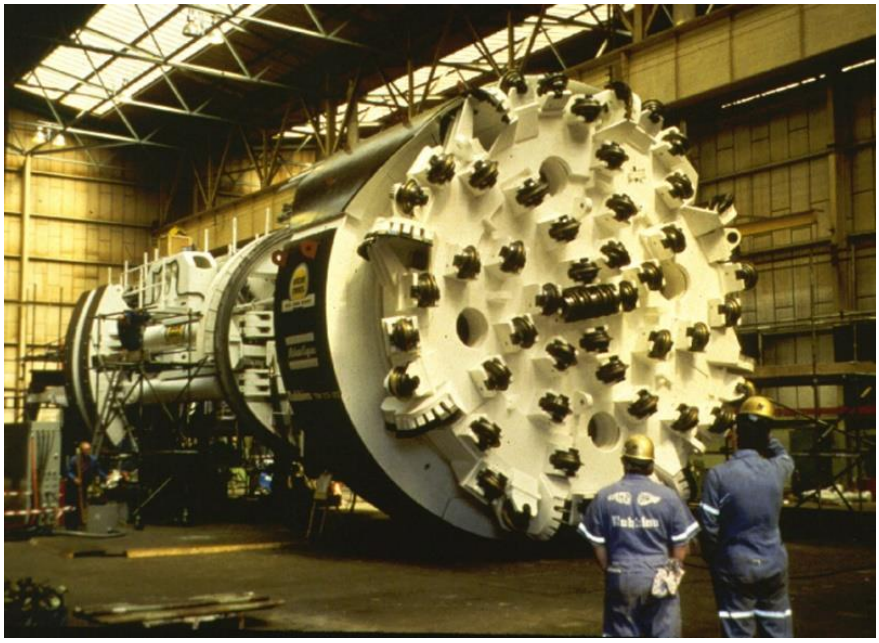

Figure 17 – View of front 84' of the roughly 300' long Robbins single-beam hard rock TBM (Model 235-282) which was assembled in bellout at base of main access shaft of Tunnel #1.

Mapping. Over the three-year period of our engagement on this tunnel project, the senior author mapped 1.75 million ft^2 of tunnel at a scale of 1" = 10' in order to fully document the tunnel walls including lithotypes, ductile geological structure, brittle faults and joints (including orientation, width, filling type and consistency, roughness, seepage, displacement and mineral coatings), areas of bad ground requiring additional support, zones of anomalous garnet concentration and water inflows. Field checking of contacts took place incrementally and measurements were entered into a database for statistical analysis. Over 3,000 digital images, 35 mm Kodachrome slides and videos which were keyed to map stationing for documentation and future DSC claim use.

The presence of iron in the service locomotive tracks, metal piping, ductwork, and the conveyor system precluded the use of a Brunton compass for standard strike-and-dip measurements. After discussions with our dear friend Scotty (Geologist, NYC DEP), we constructed a laser-pointer leveling device that was able to accurately measure the strike of features with respect to the surveyed tunnel trend (Figure 18). By climbing up on the piping of the tunnel wall and having a clear view of the other wall, features such as faults, foliation, and dikes were relatively easy to view and trace across the crown using this device. A bubble level was used to hold horizontal both ruler sections on the feature to be measured and laser pointer was used to sight the same feature on the other wall. In this way one could measure the angle made between the strike of the feature with respect to the surveyed tunnel invert centerline trend.

Great care was taken to properly calibrate the device to the centerline trend in the various curves of the tunnel. Dips were measured using a Brunton compass and checked by calculation from the field maps; strikes were also checked from the field maps. By the end of this phase an upgraded mylar-and-ink field map was produced for each 100' section of the tunnel (Figure 19.)

Figure 18 – In-house mechanism used for measuring strike of features exposed on both tunnel walls at springline and comparing to surveyed invert orientation. Dips were measured using Brunton compass and verified by standard cartographical calculations from map geometries.

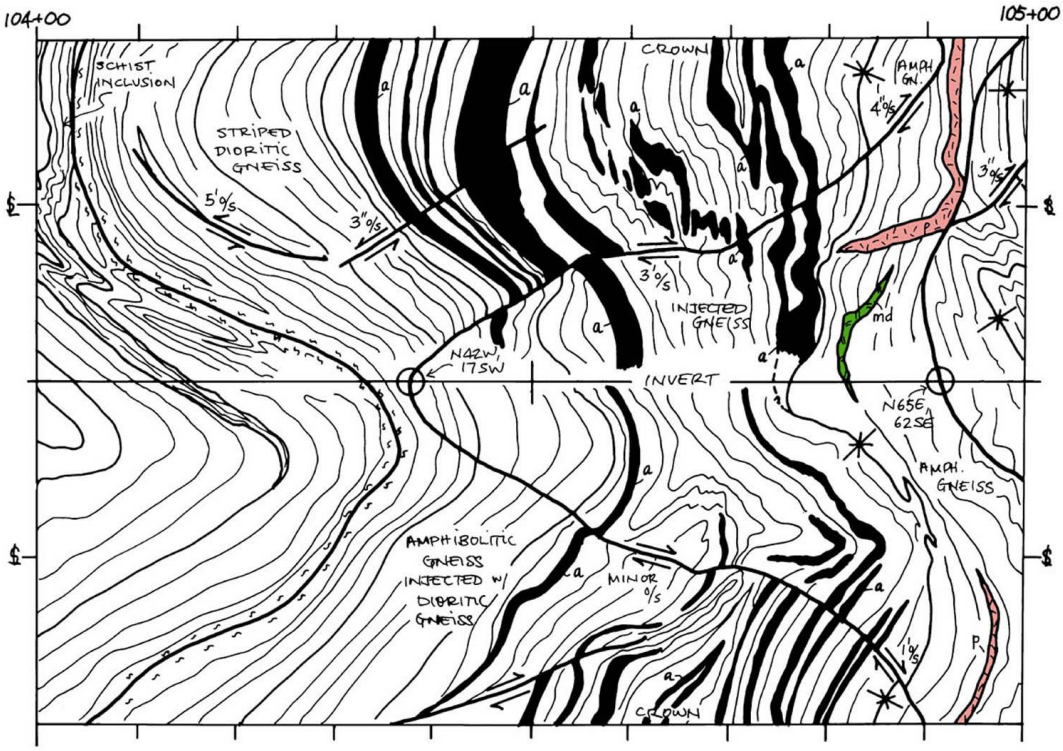

Figure 19 – Geological map of Tunnel #1 shows granulite-facies amphibolite gneiss and younger dioritic orthogneiss cut by pegmatite (p) and a mafic dike (md). The amphibolitic gneiss is locally sheared but clearly occurs as inclusions in the dioritic gneiss. The tunnel invert is shown along the center of the map and the tunnel walls curl upward into a cylinder to join at the crown. The position of the tunnel springline is shown at the map edge. This map, one of 250 in the unpublished Tunnel #1 Map Portfolio, records 100' of the tunnel. A low-angle reverse fault oriented N42°W, 17°SW cuts the invert at Station 104+38 (tunnel invert bearing is N22°E). A younger N65°E, 62°NE brittle fault cuts the invert at Station 104+91. Original map scale 1" = 10'; tunnel diameter 23' 2".

Internal rock fabrics (gneissic layering) and faults were remeasured using oriented rolled mylars of the individual maps utilizing a Brunton compass as shown in Figure 20. Such measurements disclosed that the gneissic fabric of Tunnel #1 was not in a favorable orientation for efficient TBM mining. Although the pre-bid data indicated a NE-trending steep-SE dipping rock foliations our stereonet analysis of the as-built gneissic layering between Stations 4+00 and 254+00 demonstrated that 26 of 235 poles (11%) indicated subhorizontal layering (Figure 21). Overall 64 poles (27%) showed gentle dips of less than 30°. Thus, subhorizontal to gently dipping rock fabrics underlie broad tracts (38%) of Tunnel #1. The structural grain of Tunnel #1 presented an unfavorable rock fabric orientation for productive TBM mining.

Figure 20 – Strike and dip of planar features were remeasured by sighting and compared to tunnel measurements from rolled map mylars aligned with respect to true north using a Brunton compass outdoors. Liquid refreshments stored in the cooler were enjoyed after the measurements were made, compared to map data and recorded.

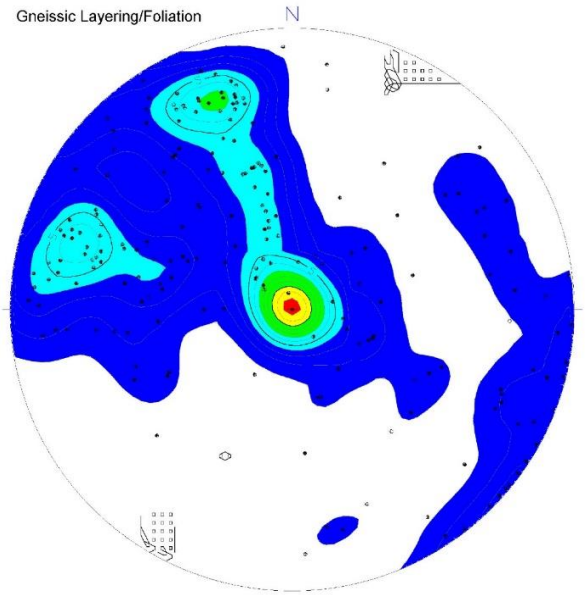

Figure 21 – Subhorizontal clustering of stereonet poles (27%) together with anticipated NNE- and ENE-strike and steep SE dips of gneissic layering/foliation (n = 254).

Petrographic Analysis. Petrography is one of the basic tools used extensively in geological analysis of crystalline rocks as it allows for identification of minerals, mineral crystal textures and metamorphic paragenesis. The process involves collection of rock samples or pieces of rock core and precise preparation of petrographic slides. The slides are 30-micron thick slices of rock sandwiched between two pieces of glass (base slide and a thinner cover slip) which together form a rock "windowpane" held together by epoxy of known optical index. In conjunction with geological mapping, metamorphic rocks reveal their structural and metamorphic history and in the case of Tunnel #1, proved that the rocks were not schist or granofels of the Hartland Formation (Figure 22).

Figure 22 – View of typical interlayered Hartland schist and granofels from an exposure at the SE part of Central Park in New York City. (Digital image taken 04 April 2003.)

Compare the rock textures shown below between foliated rocks of the anticipated Hartland Formation (Figure 23A) and a leucocratic orthogneiss found in Tunnel #1 (Figure 23B). Proper petrographic analysis would have alerted bidders to this lithologic departure from pre-bid anticipation but sadly, little competent petrographic work was conducted pre-bid on this job.

Alignment Borings. Typical core logs include information on fracture density, recovery, lithology, and sometimes the nature of fracture surfaces. Statistical studies on the borings should include recording detailed lithologic, mineralogic, and petrographic characteristics by a trained professional geologist. Integrated research on the actual core should be targeted at the depth of the tunnel horizon but comparative analysis outside the tunnel horizon should better identify possible changes that could result in surprises during actual tunneling. All of the core should be examined by the same geologist to establish consistency and core logging by drillers without

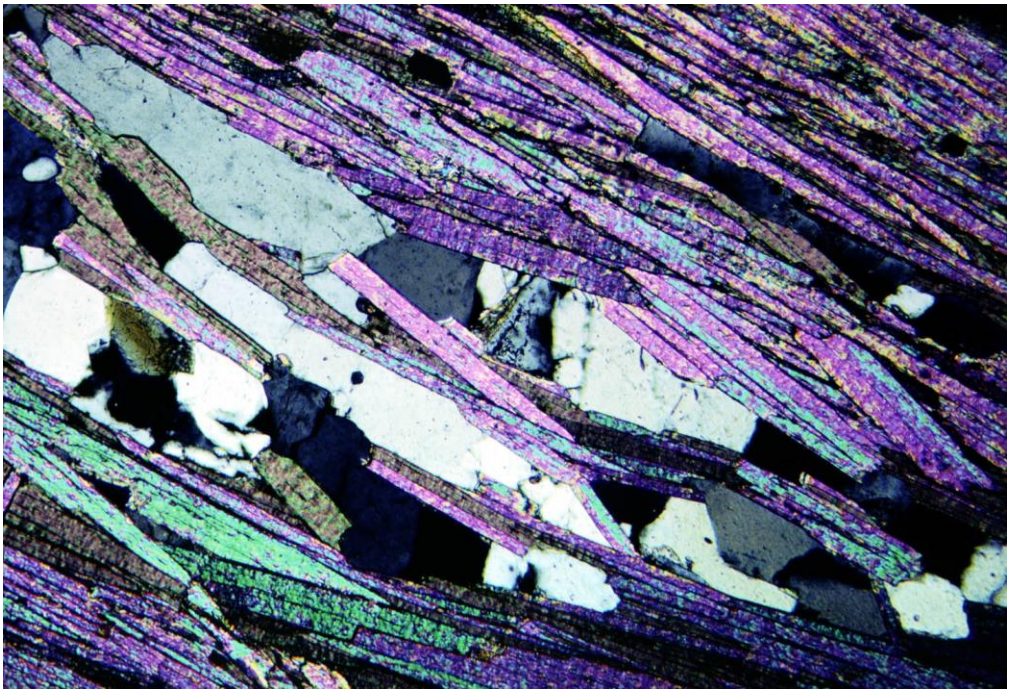

Figure 23A – Photomicrograph in crossed nicols of aluminous Hartland schist (Sample N403-1; World Financial Center site, lower Manhattan). The section shows fine-textured lenticular quartz and minor plagioclase separated by aligned muscovite and minor biotite (highly colored crystals). Such directional mineral growth results in a penetrative micaceous foliation that splits readily because of the parallelism of relatively soft mica flakes.

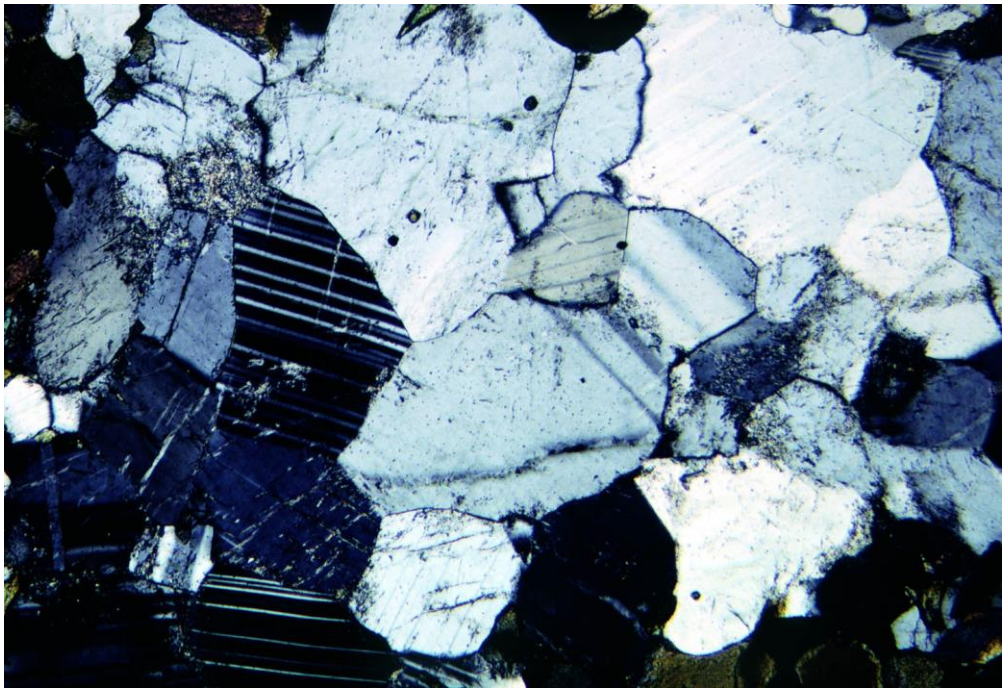

Figure 23B – Photomicrograph in crossed nicols of Tunnel #1 leucocratic orthogneiss (Sample Q085; Station 159+80) showing granoblastic intergrowth of plagioclase and minor quartz. Note the granular texture, the stable 120° grain boundaries of the interlocking plagioclase, and the lack of any penetrative foliation. Both photomicrographs of Figure 23 are 2 mm across.

professional degrees in geology or geological engineering should not be relied upon without careful rechecking. In particular, anomalous lithologies are the common cause of changed condition losses in underground work. Professional geologists are more likely to accurately identify anomalous lithologies – many examples of misidentified rock types have resulted in lost time and delays related to differing site conditions. After careful mapping of the tunnel a comparison between lithotypes depicted in the borings at the tunnel horizon were clearly misleading in identifying the proportion of various lithologies in Tunnel #1 which in this case resulted in an improper choice of TBM for the tunnel drive (Figure 24).

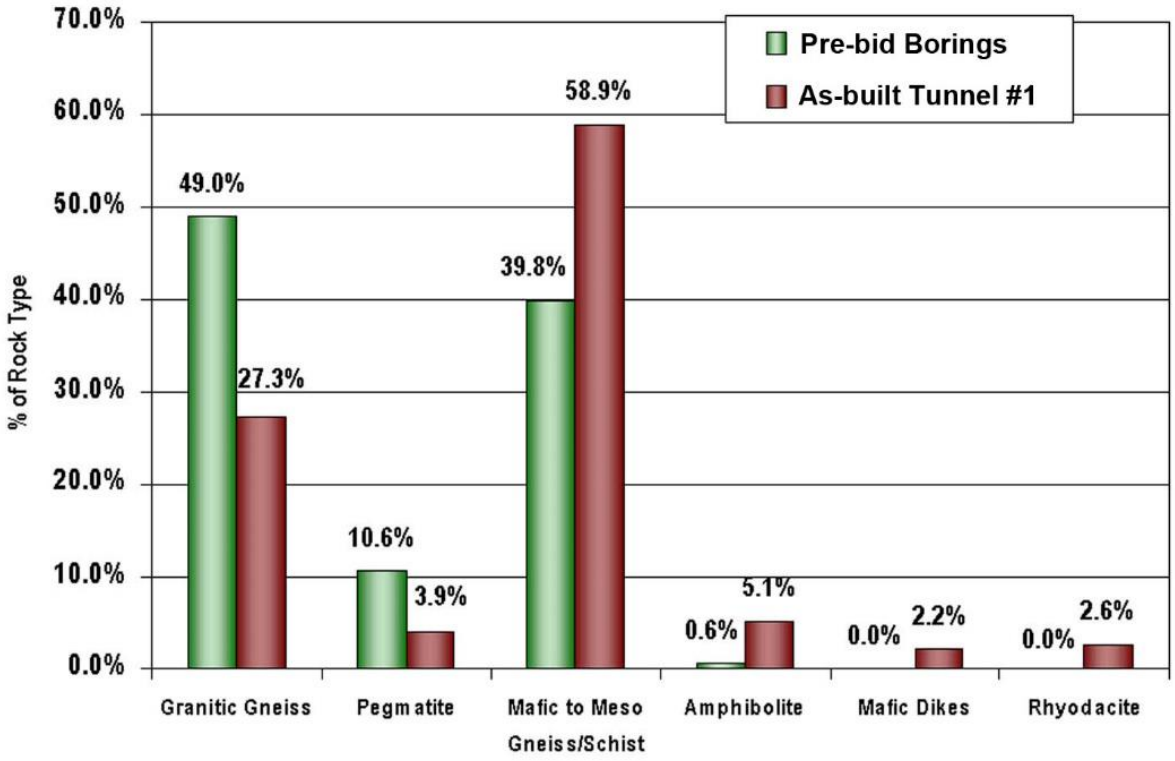

Figure 24 - Comparative bar graph showing the disparity between lithotypes identified by examining pre-bid borings (green) vs. those found to occur in a tunnel horizon by as-built mapping (red). Note the difference in the relative proportion of granitic and pegmatitic (felsic) rocks vs. the mafic, amphibolitic, and mesocratic (mafic and intermediate) rocks and the presence of unanticipated rocks of rhyodacite affinity. This compositional variation from pre-bid anticipation proved an impediment to efficient mining. (Adapted from Merguerian and Ozdemir, 2003.)

Density Analysis. Overlooked by many investigators, the density or specific gravity of rocks is a simple and useful litmus test for predicting TBM penetration. Higher density rocks are less penetrable simply because they tend to contain dense and/or hard minerals such as garnet, pyroxene, and aluminosilicate minerals such as sillimanite and kyanite. Density is readily measured using simple, inexpensive apparatus (Merguerian 2005a). A density profile along the tunnel alignment can help predict variation in density over a planned TBM expedition and can efficiently identify anomalous zones or trends in rock mass properties (Figure 25).

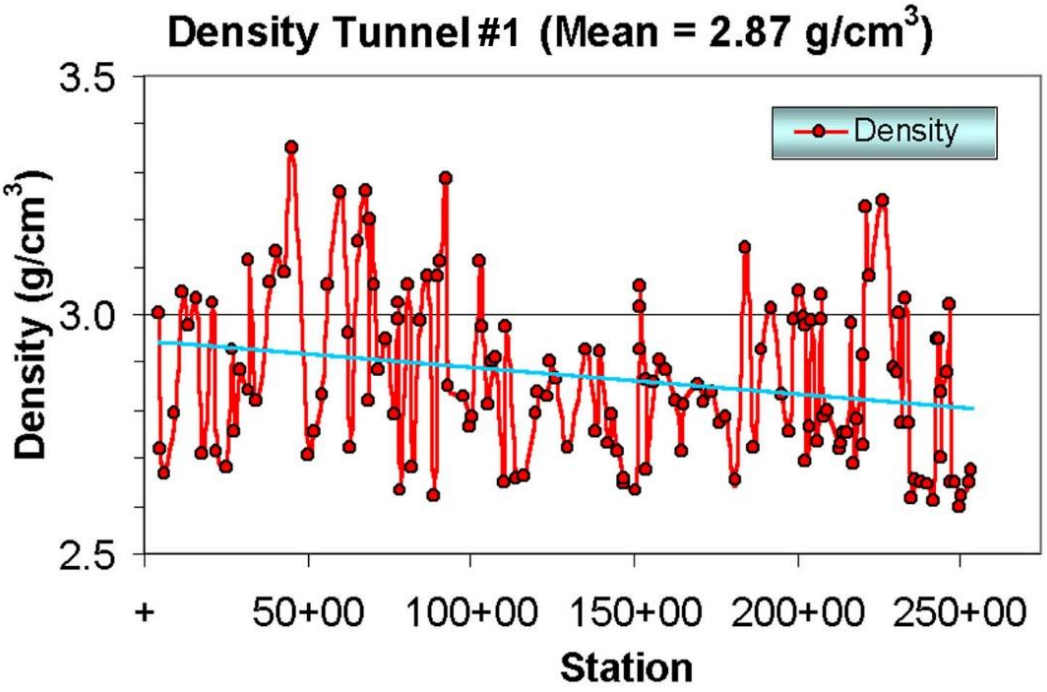

Figure 25 – Rock mass density variation as compiled from sawn slabs from 161 samples collected during as-built mapping of Tunnel #1, NYC. The graph indicates that the bulk density of the tunnel varied from 2.62 to 3.35 gm/cm^3 and that density decreased slightly toward the higher stations (sloping blue line) as shown by the mapping. The mean density (2.87 g/cm^3) was in keeping with the lithotype analysis (See Figure 24.) that indicated that more intermediate- to mafic lithologies were penetrated in the tunnel by comparison to what the pre-bid borings indicated. Typical schist and granofels which constitutes the Hartland Formation should have averaged about 2.55 g/cm^3. (Adapted from Merguerian and Ozdemir 2003.)

Penetration Rate. Average TBM penetration rates of <2 m/hour were encountered in Tunnel #1 during excavation rather than the 3m/hour anticipated. Despite the fact that pre-bid documents provided by the owner indicated that schist, granofels and amphibolite of the Hartland Formation was anticipated along the tunnel alignment, as-built mapping, structural, lithologic, and petrographic studies showed that the rocks of Tunnel #1 consisted of orthogneiss of leucocratic, mesocratic, and melanocratic composition. These metaigneous rocks developed coarse-textured fabrics during primary granulite facies metamorphism (Figure 26A) and largely retained their anhydrous, poorly foliated character during subsequent high-grade deformation and retrograde metamorphism. Indeed, the secondary pulse of high-grade metamorphism resulted in replacement growth of garnet necklaces and hornblende reaction rims at the expense of coarse-textured primary orthopyroxene, clinopyroxene, and plagioclase (Figure 26B).

Lacking a penetrative foliation, the coarse-textured granoblastic rock texture and extraordinary garnet content of up to 50% in some zones that underlie ~11% of the entire tunnel (Figures 27A, B; Table 1) together proved an impediment to efficient TBM chip production and resulted in bimodal production of rock powder (excessive fines) and large blocks that choked TBM grizzlies and damaged outgoing conveyor belt systems (Merguerian and Ozdemir 2003).

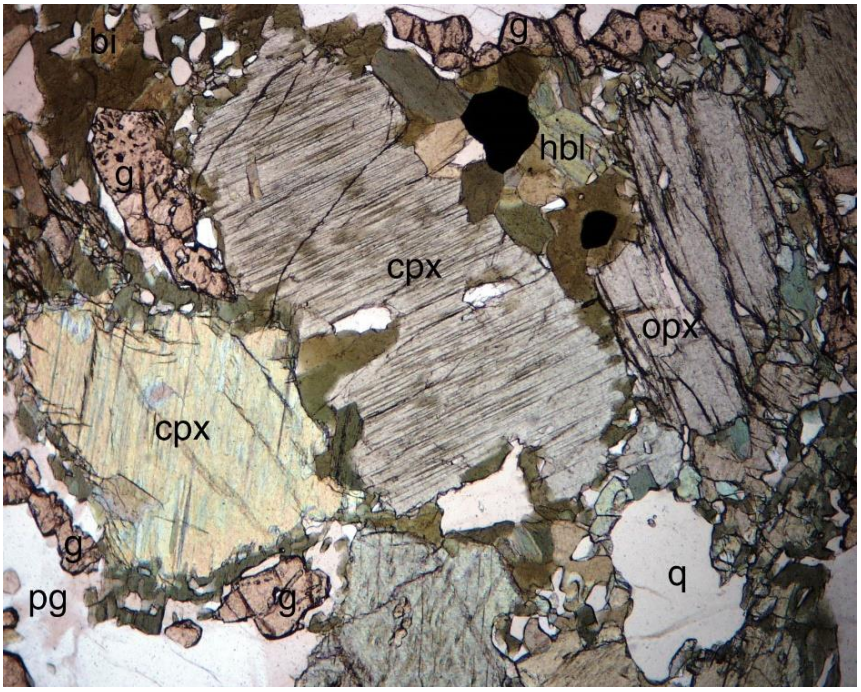

Figure 26A – Photomicrograph in plane-polarized light of Tunnel #1 mafic gneiss showing coarse-textured granulite facies texture in the form of partly recrystallized orthopyroxene (opx), clinopyroxene (cpx), and primary garnet (g). Quartz = q. Note the thin overgrowths of hornblende (hbl), granular garnet (g) and biotite (bi), the result of secondary metamorphic recrystallization. (Sample Q114; Station 15+90; 2 mm field of view.)

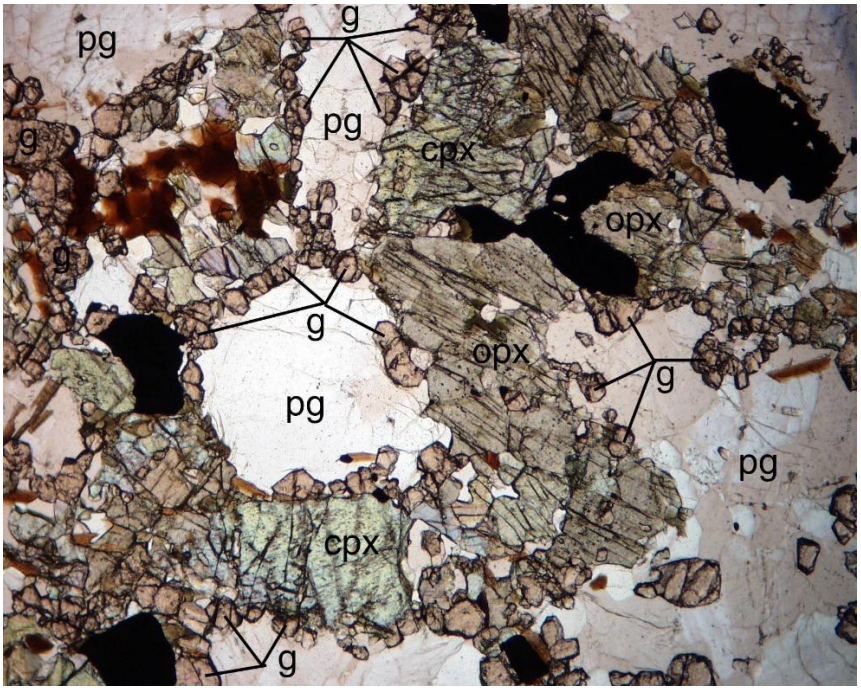

Figure 26B – Photomicrograph in plane-polarized light of mesocratic gneiss showing "garnet necklace" structure. Note the semi-circular patches of high relief garnet. This replacement texture results from the production of garnet and hornblende reactions rims adjacent to primary coarse-textured orthopyroxene, clinopyroxene, and plagioclase during secondary metamorphism. Same notation as above. (Sample Q146; Station 80+64; 2 mm field of view.)

A. **B.**

Figures 27A, B – Views of two of the 32 garnet zones mapped in Tunnel #1 showing the anomalously high concentration (up to 50%) of dense garnet that defines such zones. Highlighted in yellow on Table 1 (below) the garnet zones 9 (A.) and 21 (B.) were produced during phases of granulite- followed by upper-amphibolite facies metamorphism as detected in the petrographic analysis of mineralogy and rock mass textures.

The term garnetiferous appears on nearly every page of the pre-bid boring logs but no percentages are given. Most petrologists would use the term garnetiferous for rocks with a trace to 3%. At higher percentages, the occurrence of garnet is indeed of scientific interest. Yet, no consensus exists on the quantitative use of the term garnetiferous. Clearly the effect of garnet would vary in "garnetiferous areas" depending upon volume percent of the hard mineral. In our view, the entire tunnel is garnetiferous (5% garnet or less) and we regard this as a reasonable baseline. Yet, some areas of Tunnel #1 are so enriched in garnet (30%-50%) that broad use of the term garnetiferous is in fact misleading. Indeed, such high garnet enrichment would be termed an "ore deposit" in many parts of the world.

During TBM mining the importance of garnet hinges on the extreme hardness and high density of the mineral (Hardness 6.5 to 7.5 on Mohs' scale; Density 3.1 to 4.3 g/cm^3). The garnet is commonly found along with quartz (another abrasive mineral; hardness 7 on Mohs' scale) and can occur as finely disseminated garnet, garnetiferous layers a few feet thick, as lenticular lenses, and in highly laminated areas forming broad zones up to 263' long in the tunnel. Garnet is also found in high concentrations within amphibole+pyroxene bearing rocks as garnet+plagioclase segregations. In thin section, thin zones of garnet rim areas of relict orthopyroxene plus clinopyroxene, the product of secondary metamorphism. (See Figure 27B.) In Tunnel #1, the high degree of metamorphism (lower granulite facies) promoted the growth of garnet and denser mineral phases including orthopyroxene and clinopyroxene. Note that granulite facies metamorphism is not widely recognized in this area of NYC.

Geochemistry and Geochronology. The final nail in the coffin for support of a DSC claim was produced when samples were geochemically analyzed and dated using U-Pb methods on zircon (Brock, Brock and Merguerian 2001). The chemical affinity between the Tunnel orthogneisses and Fordham Gneiss is expressed in several ways, including the range of rock compositions present, the tectonic affinities of both the mafic and felsic rock types and geochemical traits

Anomalous Garnet Concentrations, Layers, Lenses, and Laminae					
Tunnel #1					
Tunnel Station		**Length**	**Garnet**	**Field Description**	**Samples (Q-)**
Start	**End**	**(Feet)**	**Zone No.**		
27+45	27+80	35	**1**	Garnet layer a few feet thick in migmatitic mafic gneiss, LW only	120
36+18	37+70	152	**2**	Garnet layers and laminae in injected mafic gneiss	
45+00	46+48	148	**3**	Garnetiferous mafic schist, gneiss and amphibolite	128
53+87	54+80	93	**4**	Two garnetiferous layers a few feet thick in mafic gneiss	131A, B
68+03	68+50	47	**5**	Garnetiferous zone in mafic gneiss, RW only	137, 138
68+78	69+84	106	**6**	Garnetiferous mafic schist, gneiss and amphibolite	139
70+27	70+78	51	**7**	10' thick garnet layer in mafic gneiss, schist, and amphibolite	140
71+01	71+18	17	**8**	Thin garnet lenses in mafic orthogneiss	
77+75	79+10	135	**9**	Broad zone of garnetiferous layers, lenses, and laminae	08, 144, 145
95+82	96+22	40	**10**	Garnetiferous leucosome in mafic gneiss, LW only	
96+77	99+25	248	**11**	Broad zone of garnetiferous mafic gneiss, schist, and amphibolite	153
100+13	102+46	233	**12**	Broad zone of garnetiferous mafic gneiss, schist, and amphibolite	155
103+43	103+62	19	**13**	Laminated garnet zone in mafic gneiss, schist, and amphibolite	
104+95	105+43	48	**14**	Laminated garnet zone in mafic gneiss, schist, and amphibolite	158
106+50	108+70	220	**15**	Broad zone of garnetiferous mafic gneiss, schist, and amphibolite	11
109+30	109+35	5	**16**	Blocks of garnetiferous gneissic rock in shear zone	
111+35	111+45	10	**17**	Laminated garnetiferous zone in mafic gneiss, LW only	
123+55	123+70	15	**18**	Laminated garnetiferous zone in mafic gneiss	101
151+80	152+20	40	**19**	Garnetiferous biotite schist and gneiss in contact with dacite	89A, B; 90A, B
171+15	173+78	263	**20**	Broad zone of highly garnetiferous migmatitic mafic rocks	80A, B
175+53	176+45	92	**21**	Broad zone of highly garnetiferous migmatitic mafic rocks	78
180+75	181+48	73	**22**	Garnet lenses and laminae in mafic schist, gneiss, and amphibolite	76
183+10	183+57	47	**23**	Garnet layer and laminae in mafic schist, gneiss, and amphibolite	
183+98	184+57	59	**24**	Garnet layer in mafic schist, gneiss, and amphibolite	75A, B
198+26	198+35	9	**25**	Sheared and rotated block containing garnet layers, RW only	
199+94	201+00	106	**26**	Garnetiferous layers in sheared mafic gneiss	68
201+80	202+05	25	**27**	Garnetiferous layer in mafic gneiss, RW only	14
207+18	207+95	77	**28**	Zone of garnet with layers, lenses, and laminae in mafic gneiss	20, 21
221+12	221+95	83	**29**	Thin garnet layers in mafic gneiss, schist, and amphibolite	33A, B
225+07	225+38	31	**30**	Garnetiferous granitoid at mafic gneiss/orthogneiss contact	
229+72	229+97	25	**31**	Garnetiferous zone in mafic gneiss and schist	
231+25	232+36	111	**32**	Laminated garnetiferous zone in mafic gneiss	38A, B
TOTAL ====>		**2663**	**Linear Feet of Tunnel #1 with Highly Garnetiferous Rocks = (2663/25035) = 10.64%**		

Table 1 – Compilation of anomalous garnetiferous zones of Tunnel #1 showing that excessive garnet concentrations underlie ~11% of the tunnel which resulted in untimely TBM cutter wear and the production of excessive fines. Petrographic analysis indicated that garnet production was the result of both primary granulite facies metamorphism and secondary upper amphibolite facies metamorphism that effected the terrain. Highlighted zones (9, 21) are shown above in Figures 27A and 27B.

unique to each suite of rocks. Comparative trace-element chemistry utilizing Zr/TiO2 vs. Nb/Y verified that the gneisses of Tunnel #1 were metaplutonic rocks and unlike the metasedimentary and metavolcanic lithotypes of the Hartland Formation. Tectonic affinity diagrams utilizing Rb vs. Y+Nb for leucocratic rocks and Th/Ta vs. La/Ta for melanocratic rocks both showed overlap

between Tunnel #1 orthogneisses and the Fordham Gneiss but showed no correlation with Hartland rocks forcing the conclusion that the pre-bid documents misled bidder expectation.

Geochronologic studies were performed by an outside laboratory on two samples of Tunnel #1 tonalitic gneiss. The gneisses shared similar zircon populations. An inherited component, estimated in the range 1,070-1,092 Ma, is present and most of the zircons are ~ 1.0 Ga in age. This is the similar to an age found among zircons of the Fordham Gneiss by Grauert and Hall (1973) again verifying that the Tunnel #1 gneiss could not be Hartland.

Tunnel #1 Summary

The as-built Tunnel #1 horizon exposes rocks that are clearly not the Paleozoic Hartland Formation of metasedimentary parentage. Rather, they proved to be Grenvillian migmatitic gneiss correlative with the Proterozoic Fordham Gneiss. During high-pressure granulite facies metamorphism former plutonic igneous rocks transformed into dense, coarse- to medium-textured orthogneiss (metaplutonic rocks) consisting of interlocking crystals of plagioclase, clino- and orthopyroxene, and primary garnet. The microscope showed that a penetrative primary foliation never developed in the rocks because the deep-seated metamorphic conditions precluded the growth of hydrous minerals (mica and amphibole), both foliation-producing phases. Rather, a granoblastic texture developed (See Figures 23B and 26A, B) which consisted of interlocking plagioclase, intergrown anhydrous mafic minerals and primary garnet. A second phase of presumable Taconian upper amphibolite facies metamorphism produced granoblastic fabrics with domanial growth of amphibole, biotite, and "new" garnet but the "older" granulite textures survived producing a tough rock mass that resisted efficient TBM chip production.

Extensive rock testing and TBM performance evaluation studies have provided a correlation between machine performance and natural geologic rock mass properties. The reduced TBM penetration encountered in the construction of Tunnel #1 was caused by higher than anticipated rock strength, adverse direction of rock layering and higher rock toughness brought about by grain interlocking and a high degree of anhydrous recrystallization, the results of their high-pressure granulite facies metamorphic history (Merguerian and Ozdemir 2003).

As a result of their metamorphism the rocks developed zones of unusually pronounced garnet content. The petrographic analysis also showed that the entire tunnel was garnetiferous with unusual garnet concentrations. Together, these textural and mineralogic properties result in rock mass "toughness" and high overall density. Indeed, the gneissic rock mass penetrated in Tunnel #1 possessed lithologic properties (texture, anhydrous mineralogy, lithology, density, homogeneity, lack of penetrative foliation, and abundant gently dipping fabric orientations) that collectively inhibited efficient TBM mining. In addition, blocky ground conditions resulted from intersecting fault sets (Merguerian 2002, 2015) and from fracture patterns unique to a suite of rhyodacite dikes hitherto unknown in the NYC area (Merguerian 2001).

The lessons learned from the Tunnel #1 experience include the recognition that a proper Baseline Geotechnical Report can minimize the pre-bid risks in any subsurface construction effort. In addition to identifying risk in the pre-bid stage, as-built investigations by geologists can define the rock mass conditions, mitigate risk and help eliminate wasteful DSC claims.

References Cited

Bennington, J Bret, and Merguerian, Charles, 2007, Geology of New York and New Jersey: Physical Geology Textbook Supplement, 24 p.: in Essentials of Geology with Geology of New York and New Jersey: Thomson Brooks/Cole, 510 p.

Brock, Pamela Chase; Brock, Patrick W. G.; and Merguerian, Charles, 2001, The Queens Tunnel Complex: a newly discovered granulite facies Fordham orthogneiss complex that dominates the subsurface of western Queens: p. 1-8 *in* Hanson, G. N., *chm*., Eighth Annual Conference on Geology of Long Island and Metropolitan New York, 21 April 2001, State University of New York at Stony Brook, NY, Long Island Geologists Program with Abstracts, 128 p. http://www.geo.sunysb.edu/lig/Conferences/abstracts-01/brock-3/PCBetal2001.htm

Donn, W. L., and Shimer, J. A., 1958, Graphical methods in structural geology: Appleton-Century-Crofts, Inc., NY, 180 p.

Grauert, B., and Hall, L. M., (1973) Age and origin of zircons from metamorphic rocks in the Manhattan Prong, White Plains area, southeastern New York: Carnegie Institute of Washington, Annual Report of the Director, Department of Terrestrial Magnetism (1972-73), 293-297.

Merguerian, Charles, 1994, Stratigraphy, structural geology, and ductile- and brittle faults of the New York City area, p. 49-56 *in* Hanson, G. N., *chm*., Geology of Long Island and metropolitan New York, 23 April 1994, State University of New York at Stony Brook, NY, Long Island Geologists Program with Abstracts, 165 p.

Merguerian, Charles, 2001, Young rhyodacite dikes found in the Queens Tunnel, beneath Woodside, Queens: p. 9-19 *in* Hanson, G. N., *chm*., Eighth Annual Conference on Geology of Long Island and metropolitan New York, 21 April 2001, State University of New York at Stony Brook, NY, Long Island Geologists Program with Abstracts, 128 p. http://www.geo.sunysb.edu/lig/Conferences/abstracts-01/Merguerian-dikes/Merguerian-dikes-abst.htm

Merguerian, Charles, 2002, Brittle Faults of the Queens Tunnel Complex, NYC Water Tunnel #3: p. 63-73 *in* Hanson, G. N., *chm*., Ninth Annual Conference on Geology of Long Island and metropolitan New York, 20 April 2002, State University of New York at Stony Brook, NY, Long Island Geologists Program with Abstracts, 116 p.

Merguerian, Charles, 2005a, Geological controls on effective hard-rock TBM tunneling in crystalline terrains: *in* 84th Annual Meeting, 9-13 January 2005, Compendium of Papers CD-ROM, Transportation Research Board of the National Academies, 11 p.

Merguerian, Charles, 2005b, Lithologic and structural constraints on TBM tunneling in New York City (NYC), p. 704-724 *in* Hutton, John D. and Rogstad, W.D., *eds.*, Rapid Excavation and Tunneling Conference, 2005 Proceedings Society of Mining, Metallurgy, and Exploration, 1371 p.

Merguerian, Charles, 2008a, Evaluating geological controls on hard rock excavation, New York City, NY: *in* Proceedings, Manhattan On the Rocks, American Society of Civil Engineers, Metropolitan Section, 08 May 2008, 31 p.

Merguerian, Charles, 2008b, Geological controls on means and methods of hard rock excavation, New York City, NY: p. 79-109 *in* Gorring, M. L., ed., Environmental and Engineering Geology of Northeastern New Jersey, Geological Society of New Jersey, XXV Annual Conference Proceedings, 17 October 2008, 111 p.

Merguerian, Charles, 2015, Review of New York City bedrock with a focus on brittle structures; *p. 17-67 in Herman, G. C. and Macaoay Ferguson, S., eds.*, Geological Association of New Jersey Guidebook, Neotectonics of the New York Recess, 32nd Annual Conference and Field Trip, Lafayette College, Easton, PA, 214 p.

Merguerian, Charles; and Merguerian, J. Mickey, 2012, Structural geology and metamorphism of the Inwood Marble, NYC, NY: Geological Society of America Abstract # 199974, Abstracts with Programs, v. 44, no. 2, p. 73.

Merguerian, Charles; Merguerian, J. Mickey; and Cherukupalli, Nehru, E., 2011, Stratigraphy, structural geology and metamorphism of the Inwood Marble Formation, northern Manhattan, NYC, NY: *in* Hanson, G. N., *chm.*, Eighteenth Annual Conference on Geology of Long Island and Metropolitan New York, 09 April 2011, State University of New York at Stony Brook, NY, Long Island Geologists Program with Abstracts, 19 p.

Merguerian, Charles; and Ozdemir, Levent, 2003, Rock Mass Properties and Hard Rock TBM Penetration Rate Investigations, Queens Tunnel Complex, NYC Water Tunnel #3, Stage 2: p. 1019-1036 *in* Robinson, R.A. and Marquardt, J.M., *eds.,* Rapid Excavation and Tunneling Conference, 2003 Proceedings Society of Mining, Metallurgy, and Exploration, 1334 p.

Merrill, F. J. H., and others, 1902, Metamorphic crystalline rocks of the New York City quadrangle, *in* Merrill, F. J. H.; Darton, N. H.; Hollick, Arthur; Salisbury, R. D.; Dodge, R. E.; Willis, Bailey; and Pressey, H. A., Description of the New York City district: United States Geological Survey Geologic Atlas of the United States, New York City Folio, No. 83, 19 p. (Includes colored geologic map on a scale of 1:62,500).

Olsen, P. E., 1980a, The latest Triassic and Early Jurassic formations of the Newark basin (eastern North America, Newark Supergroup): Stratigraphy, structure, and correlation: New Jersey Academy of Science Bulletin, v. 25, p. 25-51.

Olsen, P. E., 1980b, Triassic and Jurassic formations of the Newark basin, p. 2-39 in Manspeizer, Warren, ed., Field studies in New Jersey geology and guide to field trips: New York State Geological Association, 52nd, October 1980, Newark, NJ, Guidebook: Newark, New Jersey, Rutgers University, Newark College of Arts and Sciences, 398 p.

Olsen, P. E., 1980c, Fossil great lakes of the Newark Supergroup in New Jersey, p. 352-398 in Manspeizer, Warren, ed., Field studies in New Jersey geology and guide to field trips: New York State Geological Association, 52nd, October 1980, Newark, NJ, Guidebook: Newark, NJ, Rutgers University Newark College of Arts and Sciences, 398 p.

Stumm, Frederick, Chu, Anthony, Lange, Andrew D., Paillet, Frederick L., Williams, John H., and Lane, John W., Jr., 2001a, Use of advanced borehole geophysical techniques to delineate fractured-rock ground-water flow and fractures along water-tunnel facilities in Northern Queens County, New York U.S. Geological Survey Water-Resources Investigations Report 00-4276, 12 p.

Stumm, Frederick, Chu, Anthony, Lange, Andrew D., 2001b, Use of advanced borehole geophysical and techniques to delineate fractured-rock ground-water flow, faults, foliation, and fractures along the western part of Manhattan, New York: U.S. Geological Survey Open-file Report 2001-196, 46 p.

Stumm, Frederick, Chu, Anthony, and Monti, Jack, Jr., 2004, Delineation of faults, fractures, foliation, and ground-water-flow zones in fractured-rock, on the southern part of Manhattan, New York, through use of advanced borehole-geophysical techniques, U.S. Geological Survey Open-File Report 2004-1232, 212 p.

Stumm, F., Chu, A., Joesten, P.K., and Lane, J.W., 2007, Geohydrologic assessment of fractured crystalline bedrock on the southern part of Manhattan, New York, through use of advanced borehole geophysical methods: Journal of Geophysics and Engineering, Vol. 4, No. 3, 8 p.

Stumm, Frederick, Chu, Anthony, Joesten, P. K., Noll, M. L., and Como, Michael, 2013, Delineation of fractures, foliation, and groundwater flow zones of the bedrock at the Harlem River tunnel in northern New York County, New York: *in* Hanson, G. N., *chm*., Twentieth Annual Conference on Geology of Long Island and Metropolitan New York, 13 April 2013, State University of New York at Stony Brook, NY, Long Island Geologists Program with Abstracts, 12 p.